# Target Validation and Identification of Novel Boronate Inhibitors of the *Plasmodium falciparum* Proteasome

Stanley C. Xie,[†] David L. Gillett,[†] Natalie J. Spillman,[†] Christopher Tsu,[‡] Madeline R. Luth,[§] Sabine Ottilie,[§] Sandra Duffy,[∥] Alexandra E. Gould,[‡] Paul Hales,[‡] Benjamin A. Seager,[†] Carlie L. Charron,[⊥] Frank Bruzzese,[‡] Xiaofeng Yang,[‡] Xiansi Zhao,[‡] Shih-Chung Huang,[‡] Craig A. Hutton,[⊥] Jeremy N. Burrows,[#] Elizabeth A. Winzeler,[§] Vicky M. Avery,[∥] Lawrence R. Dick,[‡,∇] and Leann Tilley*,[†,∇]

[†]Department of Biochemistry and Molecular Biology, Bio21 Molecular Science and Biotechnology Institute, The University of Melbourne, Melbourne, VIC 3010, Australia

[‡]Oncology Clinical R&D, Takeda Pharmaceuticals International Co., Cambridge, Massachusetts 02139, United States

[§]Host-Microbe Systems and Therapeutics Division, UC San Diego School of Medicine, La Jolla, California 92093, United States

[∥]Griffith Institute for Drug Discovery, Griffith University, Brisbane, QLD 4111, Australia

[⊥]School of Chemistry, Bio21 Molecular Science and Biotechnology Institute, The University of Melbourne, Melbourne, VIC 3010, Australia

[#]Medicines for Malaria Venture, 1215 Meyrin, Switzerland

S *Supporting Information*

ABSTRACT: The *Plasmodium* proteasome represents a potential antimalarial drug target for compounds with activity against multiple life cycle stages. We screened a library of human proteasome inhibitors (peptidyl boronic acids) and compared activities against purified *P. falciparum* and human 20S proteasomes. We chose four hits that potently inhibit parasite growth and show a range of selectivities for inhibition of the growth of *P. falciparum* compared with human cell lines. *P. falciparum* was selected for resistance in vitro to the clinically used proteasome inhibitor, bortezomib, and whole genome sequencing was applied to identify mutations in the proteasome β5 subunit. Active site profiling revealed inhibitor features that enable retention of potent activity against the bortezomib-resistant line. Substrate profiling reveals *P. falciparum* 20S proteasome active site preferences that will inform attempts to design more selective inhibitors. This work provides a starting point for the identification of antimalarial drug leads that selectively target the *P. falciparum* proteasome.
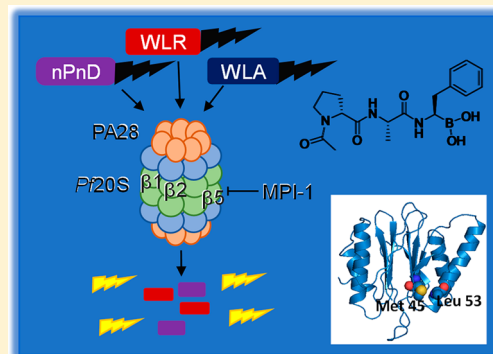
INTRODUCTION

Malaria remains a major health problem, threatening hundreds of millions of people and causing ~440 000 deaths each year.[1] Current antimalarial control is highly dependent on artemisinin-based combination therapies (ACTs), which makes the emergence of artemisinin partial resistance extremely concerning.[2−4] Decreased ACT sensitivity delays the clearance of parasites from patients and leads to clinical failure, resulting in ~50% treatment failure in regions where resistance is entrenched, compared with ~2% failure in regions where resistance is rare.[5,6] Replacement antimalarials are therefore urgently needed.

The proteasome is a multisubunit enzyme complex that is responsible for proteostasis and for regulating key processes such as the cell cycle. It has a 20S catalytic core that includes two heptameric rings of β subunits. The β1 subunit provides caspase-like activity (cleaves after acidic residues), the β2

subunit trypsin-like activity (cleaves after basic residues), and the β5 subunit chymotrypsin-like activity (cleaves after nonpolar residues).[7] In cells exposed to oxidative stress or inflammatory cytokines, three of the active constitutive proteasome subunits are replaced by "immuno" subunits to form immunoproteasomes.[8]

Proteasome inhibitors show potential for the treatment of malaria, exhibiting parasiticidal activity against asexual blood stages, including young (ring stage) intraerythrocytic parasites, as well as sexual stage gametocytes and liver stage parasites,[9−11] life stages that are resistant to most other chemotherapeutic agents. Moreover, inhibitors of the proteasome are active against both artemisinin-sensitive and -resistant parasites[12,13] and, indeed, strongly synergize
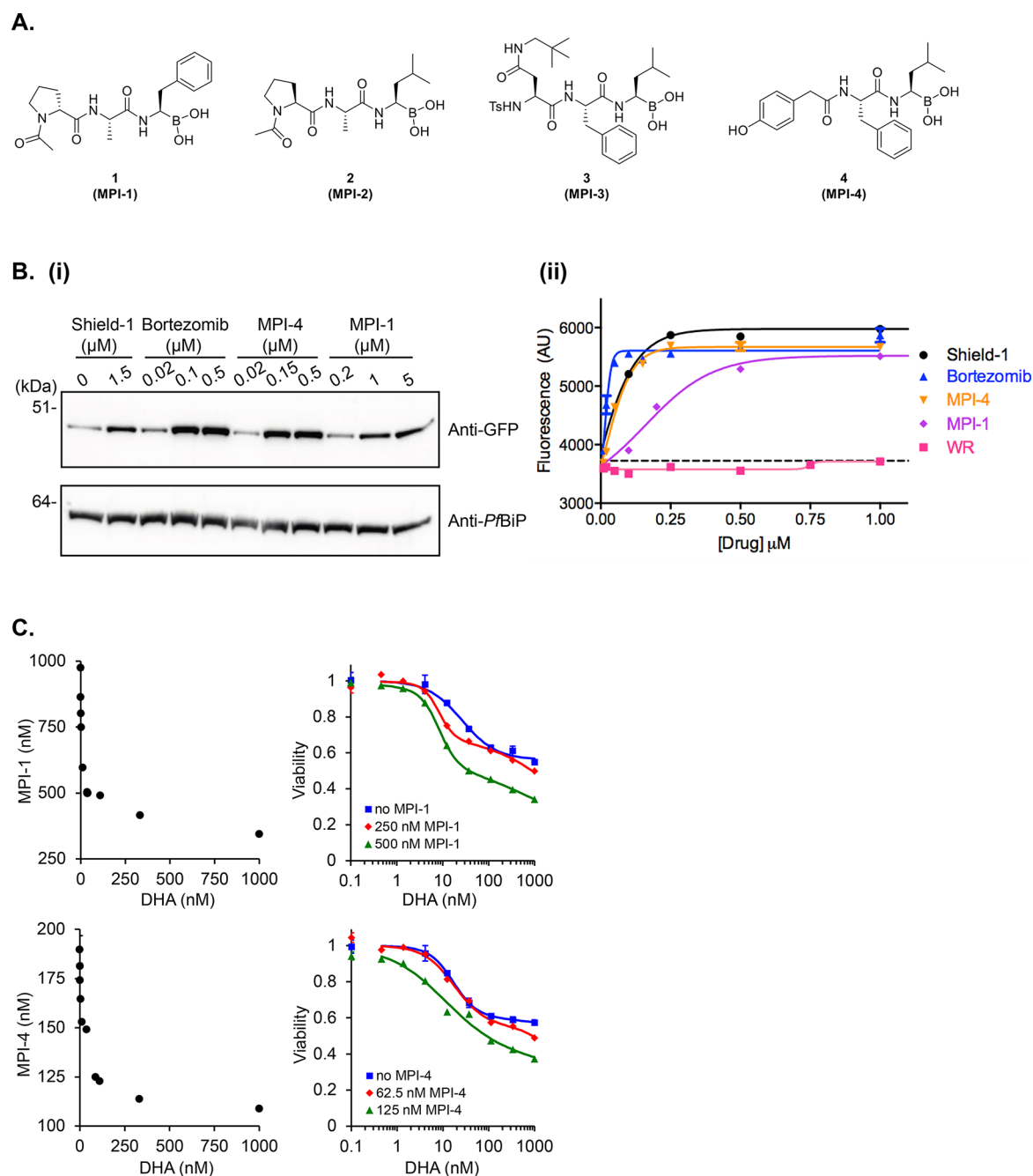
**Figure 1.** Structures, proteasome inhibition, and isobologram analysis of selected compounds. (A) Structures of MPI-1, MPI-2, MPI-3, and MPI-4 (compounds **1−4**). (B) GFP-DD transfectants were maintained in Shield-1 for 24 h before wash-out prior to setting up experiments. Trophozoites were re-exposed to Shield-1 or exposed to indicated compounds for 3 h. Results are representative of four independent experiments. (i) Cell extracts were analyzed by Western blot using anti-GFP or anti-*Pf*BiP as a loading control. (ii) GFP fluorescence measured by flow cytometry. Dotted line represents background (fluorescence of sample after washout of Shield-1). Data are the mean ± range/2 for the readings in technical duplicate from one experiment. Curves are fitted with the sigmoidal four-parameter model. (C) Isobologram analysis of the interaction of test compounds and DHA. Cam3.II (DHA resistant) parasites at very early ring stages were subjected to 3 h pulses in the presence of different combinations of DHA and test compounds. The left side of each panel presents the isobolograms for the test compound−DHA pair at the 50% LD_{50}(3 h) level. The right side of each panel shows the influence of sublethal concentrations of the test compounds (indicated in figure) on the dose−response profile of DHA. Data shown are representative of three independent experiments. Error bars, where present, correspond to the range of technical duplicates.

artemisinin-mediated killing of *P. falciparum* in culture and *P. berghei* in vivo.[11,12] To date, efforts to identify proteasome inhibitors as potential antimalarial compounds have concentrated on inhibitors with epoxyketone and vinyl sulfone warheads that bind irreversibly to the proteasome active site. A recent report examined noncovalent asparagine ethylenedi-amine (AsnEDA) inhibitors and revealed good cellular selectivity, but this class of inhibitors is not stable in vivo (half-life of ∼30 min) and thus is not active (when used alone) in a mouse model of malaria.[11] If a potent, specific, and "drug-like" proteasome inhibitor could be identified, it would be a

Scheme 1. Synthesis of MPI Pinane Esters[a]
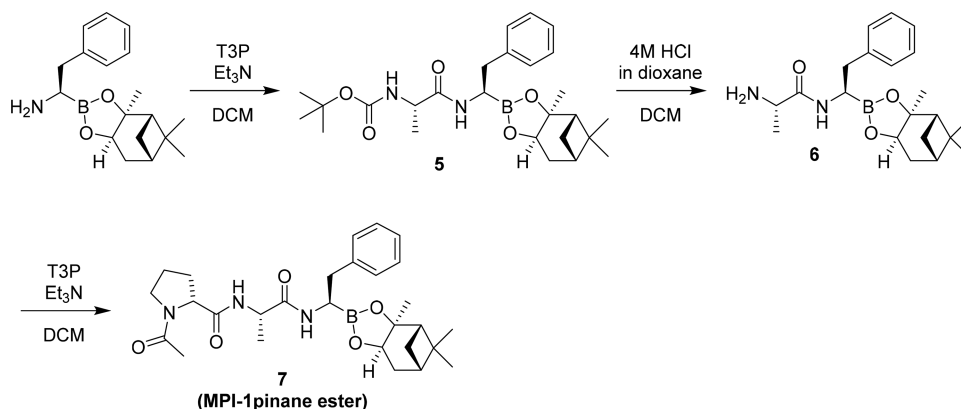
[a]Reagents and conditions: (a) Boc-L-alanine, T3P, Et₃N, DCM, room temperature, 73%; (b) 4 M HCl in dioxane, Et₂O, DCM, room temperature, 93%; (c) (R)-(+)-N-acetylproline, T3P, Et₃N, DCM, room temperature, 38%.

promising antimalarial compound in its own right and would be particularly effective in combination with artemisinins.

The reversible, covalent peptide boronate proteasome inhibitors bortezomib[14] and ixazomib[15] are used clinically to treat multiple myeloma. Ixazomib is administered orally and offers a favorable efficacy/safety profile with weekly dosing delivered as a fixed dose.[16,17] Bortezomib has been shown to have activity against *P. falciparum*,[12,18,19] although it has not been formally demonstrated that this results from inhibition of the *P. falciparum* proteasome. In this work, we used in vitro directed evolution to generate bortezomib-resistant parasites, thereby validating the β5 subunit of the proteasome as the target. We screened a boronate peptide library to identify inhibitors of the growth of cultures of *P. falciparum* and selected compounds for further characterization. We show that inhibition of β5 activity is needed for potent antiplasmodial activity but that compounds that also inhibit β2 activity remain active against bortezomib-resistant parasites. Substrate profiling points to substrate preferences that can underpin the development of inhibitors with high specificity against *P. falciparum*.

■ RESULTS AND DISCUSSION

Establishment of an Assay of *P. falciparum* 20S Proteasome Activity. Purified *Pf*20S proteasome (see characterization in Figure S1A,B) was activated using human proteasome activator complex (PA28αβ), and the activity was assessed using fluorogenic AMC-based substrates. Initial testing of a range of substrates (Figure S2A) suggested the use of Ac-nLPnLD-AMC for caspase-like activity (β1 subunit), Ac-WLR-AMC for trypsin-like activity (β2 subunit), and Ac-WLA-AMC for chymotrypsin-like activity (β5 subunit). The activity of β2 and β5 subunits was completely abrogated by 0.8 μM carfilzomib (Figure S2B), consistent with a previous report.[9] By contrast, carfilzomib exhibited only weak inhibitory effect against *Pf*20S proteasome β1 activity (Figure S2B).

To assess the level of proteasome activity contributed by the estimated human 20S proteasome contaminant (1 in 240), we compared the activity of 1 nM *Pf*20S with that of 0.005 nM human constitutive proteasome (Figure S2C). Human β1c and β2c activities were not detected, and the fluorescence signal generated from β5c activity was only 2% of that from *Pf*20S β5.

Analysis of the Activities of Selected Compounds against *P. falciparum* and Mammalian Cell Lines. Peptide boronates from the library of the Takeda Oncology Company (Cambridge, MA, USA), were screened for inhibition of the growth of cultures of *P. falciparum* (3D7).[20] Further characterization of the compounds for activity against *Pf*20S and human 20S proteasome activity led to the selection of four compounds for further investigation, namely, malaria proteasome inhibitors (MPI-1, MPI-2, MPI-3, MPI-4; compounds **1–4**), as well as bortezomib itself (Figure 1A). The pinane esters of MPI-1 to -4 (compounds **7–10**) were resynthesized and characterized in-house (see Scheme 1 and Experimental Methods).[21] Analysis of MPI-1, MPI-2, MPI-3, MPI-4 as inhibitors of the activity of purified *Pf*20S and human 20S proteasome, in fluorogenic peptide assays, revealed that they exhibit good inhibition of both β2 and β5 activities of *Pf*20S (MPI-3 and MPI-4) or more selective inhibition of β5 activity (MPI-1, MPI-2 and bortezomib) (as summarized in Table 1). MPI-3 and -4 are more active against *P. falciparum* β2 than human β2c or β2i. However, all four compounds were more active against the β1 and β5 activities of the human 20S isoforms (Table 1). While the levels of selectivity are less dramatic than in a recent study of asparagine ethylenediamine (AsnEDA) inhibitors,[11] those assays were performed in the presence of 0.5 μM WLW-vinyl sulfone, which acts synergistically with inhibitors of *Pf*20S β5.[11,13]

MPI-4 was chosen for a detailed kinetic analysis because it exhibited some selectivity for *P. falciparum* β2 compared with human constitutive β2 (β2c) (Table 1A,B). It shows very rapid and tight (K_i = 0.13 nM) binding to the human β5c but weaker affinity for *P. falciparum* β5 (K_i = 4.3 nM) (Figure S3B,D). Binding to the human β2c is very weak (K_i = 487 nM), while binding to *P. falciparum* β2 is relatively stronger (K_i = 6.4 nM) (Figure S3A,C).

Peptide boronates are covalent, slowly reversible inhibitors,[22] with bortezomib exhibiting a $t_{1/2}$ value of ~110 min for dissociation from the β5 site.[23] We found that MPI-4 exhibited a similar $t_{1/2}$ at the human β5c site (106 min, K_i = 0.1 nM) but only 2 min (K_i = 490 nM) at the β2c site (Figure S3A), indicating it is only tightly bound at the human β5c site. In contrast, MPI-4 bound to both the β2 and β5 sites of *Pf*20S with high affinity (~5 nM) and extended $t_{1/2}$ (~65 min). This indicates a key difference between the *P. falciparum* β2 and human β2c sites, potentially arising from the open con-

Table 1. Summary of Inhibitory Activities of Selected Compounds against Purified *P. falciparum* and Human 20S Proteasome[a]

(A)		
Plasmodium falciparum 20S proteasome IC$_{50}$ (μM)		
compd	β1	β2	β5
MPI-1	3.19 ± 0.04	>10	1.5 ± 0.5
MPI-2	3.0 ± 0.5	>10	2.9 ± 0.5
MPI-3	1.78 ± 0.48	0.07 ± 0.01	0.016 ± 0.002
MPI-4	0.6 ± 0.1	0.06 ± 0.01	0.010 ± 0.002
bortezomib	0.32 ± 0.08	1.6 ± 0.3	0.053 ± 0.004
(B)		
Homo sapiens 20S constitutive proteasome IC$_{50}$ (μM)		
compd	β1c	β2c	β5c
MPI-1	3.4 ± 0.9	>10	0.22 ± 0.03
MPI-2	0.32 ± 0.07	>10	0.097 ± 0.009
MPI-3	1.6 ± 0.2	0.44 ± 0.08	0.009 ± 0.002
MPI-4	0.052 ± 0.004	0.68 ± 0.06	0.0014 ± 0.0003
bortezomib	0.09 ± 0.02	1.2 ± 0.1	0.006 ± 0.001
(C)		
Homo sapiens 20S immunoproteasome IC$_{50}$ (μM)		
compd	β1i	β2i	β5i
MPI-1	0.008 ± 0.002	>10	0.028 ± 0.006
MPI-2	0.013 ± 0.002	>10	0.063 ± 0.008
MPI-3	0.029 ± 0.005	0.13 ± 0.02	0.005 ± 0.002
MPI-4	0.005 ± 0.001	0.30 ± 0.04	0.0013 ± 0.0002
bortezomib	0.005 ± 0.002	0.54 ± 0.08	0.0020 ± 0.0004

[a]IC$_{50}$ values of selected compounds against *Pf*20S proteasome (A), human constitutive proteasome (B), and immunoproteasome (C) are shown. Data represent the mean ± SEM for three independent experiments.

formation of the *P. falciparum* β2-binding pocket compared to the human proteasome,[13] which might be exploited in the development of *Pf*20S selective inhibitors.

Careful reanalysis of dose−response profiles ($n = 3$) against 3D7 parasites revealed 50% viability inhibitory concentration values of ∼0.06 μM for MPI-3, MPI-4 and bortezomib (Table 2A). MPI-1 and MPI-2 exhibited only ∼2-fold weaker parasite killing activity (Table 2A), despite their several-fold weaker activities against *P. falciparum* β5 and very poor activity against *P. falciparum* β2 (Table 1). This suggests that extended exposure to weaker inhibitors of β5 can still induce parasite killing.

To investigate the ability of the compounds to inhibit *P. falciparum* proteasome activity in cells, we made use of transfectants expressing GFP fused to a destabilization domain (DD),[24] which, when destabilized, is targeted for degradation in a proteasome-dependent manner. Addition of a protective ligand, Shield-1, stabilizes the fusion protein and prevents GFP-DD degradation, leading to an accumulation of full-length protein (as assessed by Western blotting) as well as an increase in the fluorescence signal from the GFP reporter (Figure 1Bi,ii). Inhibition of the proteasome, using bortezomib, prevented GFP-DD degradation in the absence of Shield-1, as indicated by the accumulation of the full-length protein (Figure 1Bi) and an increase in the fluorescence signal (Figure 1Bii). Treatment with MPI-4 had a similar effect, while a higher concentration of MPI-1 was needed to produce the same level of inhibition of GFP-DD degradation (Figure 1Bi,ii). These data are consistent with the novel inhibitors exerting their activity by disrupting proteasome-dependent degradation.

Mutations in a Kelch domain protein of unclear function (K13-propeller; PF3D7_1343700) are associated with decreased artemisinin sensitivity in vivo[25] and reduced sensitivity of very early ring stage parasites in a pulse assay format in vitro.[25] We examined the activity of the novel proteasome inhibitors in a 3 h pulsed exposure against a K13 mutant field strain from Cambodia (Cam3.II^{R539T}) and an isogenic line (Cam3.II^{rev}), in which the *K13* wild-type genotype has been restored and sensitivity to dihydroartemisinin (DHA) regained.[26] All compounds exhibited similar activity against K13 wild-type and mutant parasites (Table 2B). MPI-1 and MPI-2 showed relatively weaker activity than MPI-3 and MPI-

Table 2. Activity of Selected Compounds and Bortezomib against *P. falciparum* and Mammalian Cancer Cell Lines[a]

(A)				
compd	*Pf*3D7 LD$_{50}$ (72 h) (μM)	HCT116 LD$_{50}$ (72 h) (μM)	HepG2 LD$_{50}$ (72 h) (μM)	selectivity (HepG2 LD$_{50}$)/(*Pf*3D7 LD$_{50}$)
MPI-1	0.12 ± 0.01	0.79 ± 0.01	6.7 ± 3.2	56
MPI-2	0.16 ± 0.02	1.3 ± 0.3	2.4 ± 0.73	15
MPI-3	0.065 ± 0.004	0.027 ± 0.002	0.26 ± 0.06	4
MPI-4	0.061 ± 0.007	0.025 ± 0.014	0.04 ± 0.01	0.7
bortezomib	0.06 ± 0.01	0.006 ± 0.001	0.03 ± 0.02	0.5
(B)				
compd	Cam3.II^{R539T} LD$_{50}$ (3 h) (μM)		Cam3.II^{Rev} LD$_{50}$ (3 h) (μM)	
MPI-1	0.82 ± 0.06		0.9 ± 0.1	
MPI-2	1.5 ± 0.2		1.8 ± 0.2	
MPI-3	0.19 ± 0.03		0.21 ± 0.03	
MPI-4	0.16 ± 0.01		0.18 ± 0.02	
bortezomib	0.12 ± 0.02		0.18 ± 0.06	

[a](A) Analysis of toxicity against 3D7 parasites and mammalian cancer cell lines. Sorbitol-treated ring stage parasites were incubated with the compounds, and viability was assessed in the next cycle (at ∼72 h). Data represent the mean ± SEM for three independent experiments. HCT116 or HepG2 cells were incubated with the compounds for 72 h before the viability was measured. Data represent the mean ± SEM or half range for 2−4 independent experiments, each performed in triplicate (HCT116) or duplicate (HepG2). (B) Pulsed exposure analysis of inhibition of the growth and viability of artemisinin-sensitive and -resistant parasites. Synchronized early ring parasites (1−3 h p.i.) were exposed to compounds for 3 h, and viability was assessed in the next cycle. Data represent the mean ± SEM for three independent experiments.

4 in this 3 h pulse assay, suggesting a slower mode of action or a faster off-rate.

We next examined the activities (72 h exposure) of the selected compounds against a colorectal carcinoma cell line, HCT116, that is particularly susceptible to proteasome inhibitors[27] and against the human hepatoma cell line, HepG2, that has been used frequently to assess selectivity in the screening of antimalarial compounds.[11,28,29] While bortezomib exhibited 2-fold higher potency against HepG2 compared with *P. falciparum*, MPI-1 was 56 times more effective against *P. falciparum* cultures compared to the HepG2 (Table 2A). This represents a 112-fold improvement in selectivity relative to bortezomib. These data indicate that compounds that exhibit weaker binding to the human $\beta 5$ subunit (see Table 1) permit better tolerability while retaining reasonable activity against *P. falciparum*.

We have previously shown that the clinically used proteasome inhibitor, bortezomib, is a potent inhibitor of the growth of *P. falciparum* in culture and exhibits strong synergism with the clinically relevant artemisinin, DHA.[12] Similarly, both MPI-1 and MPI-4 exerted a pronounced synergistic interaction with DHA against the early ring stages of the K13 mutant isolate, Cam3.II[R539T] (Figure 1C).

In Vitro Evolution of Bortezomib-Resistant Parasites and Validation of the Inhibitor Target. In an effort to confirm that the peptide boronates exert their antiplasmodial activity via direct binding to one or more proteasome subunits and to determine the residues that are important for the inhibitory activity, we selected *P. falciparum* for resistance to bortezomib, followed by whole genome sequencing. This approach has been used successfully to identify and characterize the targets of a number of antiparasitic compounds.[30,31]

Multiple cloned lines of 3D7 were subjected to gradually increasing concentrations of bortezomib over a period of about 30 weeks. Two independent resistant lines (B1, B2) were obtained (Figure S4) and cloned by limiting dilution. The selected clones (B1a, B2a) exhibited an approximately 20-fold increase in the 50% inhibitory concentration (Table 3A). The resistance phenotype was stable to freezing and thawing of the

Table 3. Inhibitory Activity of Bortezomib and Selected Compounds against Bortezomib-Resistant Parasites[a]

| (A)	
parasite	LD_{50} (72 h) (μM)
3D7 parent	0.06 $\pm$ 0.01
3D7 B1a	1.3 $\pm$ 0.1
3D7 B2a	1.1 $\pm$ 0.1
(B)	
compd	bortezomib-resistant 3D7 B1 line LD_{50} (72 h) (μM)
MPI-1	0.23 $\pm$ 0.04
MPI-2	>2
MPI-3	0.054 $\pm$ 0.007
MPI-4	0.077 $\pm$ 0.001

[a](A) Full-cycle analysis of bortezomib inhibition of wild-type and bortezomib-resistant clones. Sorbitol-treated ring stage parasites were incubated with bortezomib for 72 h, and viability was assessed. Data represent the mean $\pm$ SEM for three independent experiments. (B) Full-cycle analysis of inhibition of bortezomib-resistant parasites. Sorbitol-treated ring stage parasites were incubated with the compounds for 72 h, and viability was assessed. Data represent the mean $\pm$ SEM for three independent experiments.

parasite clones. Whole genome sequencing was performed on the parental *P. falciparum* 3D7 clone and three independent clones (B1a,b,c; B2a,b,c) from each of the resistant lines selected with bortezomib. These six genomes yielded on average 26 million (26 191 102) reads with an average read length of 100 bp. Of these, 99.1% mapped to the *P. falciparum* reference genome (PlasmoDB version 13.0). An average coverage of 87.4% was obtained with an average of 97.7% of the genome covered by five or more reads (Table S1). Aligning each sequence as well as the drug-sensitive parent clone sequence to the reference 3D7 line revealed that each of the B1 and B2 clones had acquired a single C → A/T nucleotide variant (at Pf3D7_10, position 441,641), while the B1 line had an additional T → A variant (at Pf3D7_10, position 441,617). These changes are predicted to result in mutations in *Pf*20S $\beta 5$ (line B1, Met45Ile and Leu53Phe; line B2, Met45Ile) (Figure 2A). The data also indicate a high degree of specificity: only two other newly emerged high-quality missense variants were detected among the 138 million bases scanned. These included a Gly425Asp change in in eukaryotic translation initiation factor 2 γ subunit (PF3D7_1410600, all B2 clones) and a Gln60His variant in a predicted dicarboxylate/tricarboxylate carrier protein (PF3D7_0823900) in one B2 clone (Table S2). No obvious copy number variants (CNVs) were observed in any of the selected lines.

In the yeast and human $\beta 5$ subunit, the boron atom covalently interacts with the active site Thr1 and the interaction is further stabilized by the hydrogen bonding network between bortezomib and several closely located residues (i.e., Thr21, Gly47, Ala49, and Ala50).[22,32] The proteasome $\beta 5$ subunit in *P. falciparum* has the identical Gly47, Ala49 and Ala50 residues (Figure 2A,C). The structure of *Pf*20S has been solved using cryoEM (PDB code 5fmg).[13] As illustrated in Figure 2B and Figure 2C, the mutations are in residues that lie close to the expected bortezomib-binding pocket.[33] Met45 in the yeast and human $\beta 5$ subunits has been shown to undergo a conformational change to drive induced fit binding of bortezomib into the S1 pocket in the $\beta 5$ active site.[22,32] Of interest, a Met45Val mutation is readily selected when human cells evolve resistance to bortezomib,[33] and the equivalent Met120Ile mutant was observed in some patients under prolonged treatment with bortezomib[34] and was selected when yeast was rendered resistant to a peptide epoxyketone inhibitor with good activity against *P. falciparum*.[35]

Overlay of the *Pf*20S $\beta 5$ structure and the crystal structure of the human 20S with bound bortezomib (PDB code 5lf3) reveals close conservation of the residues lining the active site (Figure S5A). In the overlaid *Pf*20S structure, Met45 is positioned unfavorably with respect to the bortezomib P1 leucine (predicted distance 1.8 Å; Figure S5B). This indicates that, as is the case for the yeast active site,[22] Met45 would need to be repositioned for bortezomib binding. PyMol[36] was used to model the Met45Ile mutation in silico (without energy minimization). The distance between the bortezomib P1 substituent (Leu) and Ile45 in *Pf*20S $\beta 5$ is predicted to increase to 3.5 Å (Figure S5C). The increased distance and the inflexibility of the branched β-carbon of Ile45 may alter the local conformation at this site and/or inhibit the conformational changes in the S1 pocket that are needed for induced fit bortezomib binding.

Interestingly, clone B1a has an additional mutation (Leu53) in *Pf*20S $\beta 5$ and exhibits a moderately higher level of resistance

A.

Pf Beta-5: *Pf* Line B1: Met45Ile & Leu53Phe; Line B2: Met45Ile

```
Human  β5    MALASVLERPLPVNQRGFFGLGGRADLL-DLGPGS-LSDGLSLAAPGWG----------V
   Pf  β5    MVIAS---------DESFMNE--IDNLINDVEDERIDNDELEFCVAPVNVPRNFIKYAQT
             *.:**        :..*:.    :*: *:    .* *.:..   .          .


Human  β5    PEEPGIEMLHGTTTLAFKFRHGVIVAADSRATAGAYIASQTVKKVIEINPYLLGTMAGGA
   Pf  β5    QNKKLFDFHKGTTTLAFKFKDGIIVAVDSRASMGSFISSQNVEKIIEINKNILGTMAGGA
             ::   ::: :*********:.*.***.****: *::*:**.*:*:**** :********


Human  β5    ADCSFWERLLARQCRIYELRNKERISVAAASKLLANMVYQYKGMGLSMGTMICGWDKRGP
   Pf  β5    ADCLYWEKYLGKIIKIYELRNNEKISVRAASTILSNILYQYKGYGLCCGIILSGYDHTGF
             *** :**: *.:  :******:*:*** ***.:*:*::***** **. * ::.*:*: *


Human  β5    GLYYVDSEGNRISGATFSVGSGSVYAYGVMDRGYSYDLEVEQAYDLARRAIYQATYRDAY
   Pf  β5    NMFYVDDSGKKVEGNLFSCGSGSTYAYSILDSAYDYNLNLDQAVELARNAIYHATFRDGG
             .:*:***..*:::.*  ** ****.***.::* .*.*:*:::** :***.***:**.**.


Human  β5    SGGAVNLYHVREDGWIRVS-SDNVADLHEKYSGSTP------
   Pf  β5    SGGKVRVFHIHKNGYDKIIEGEDVFDLHYHYTNPEQKDQYVM
             *** *.::*::::*:  :: ::* *** :*:.
```
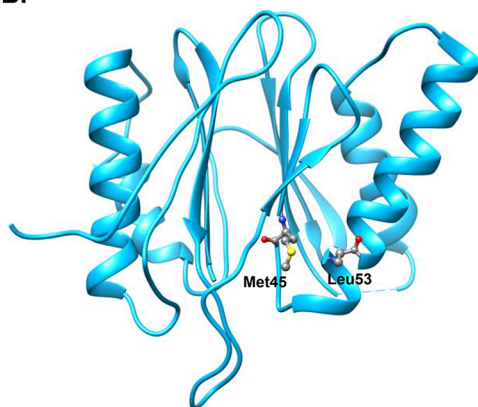
B.   **C.**
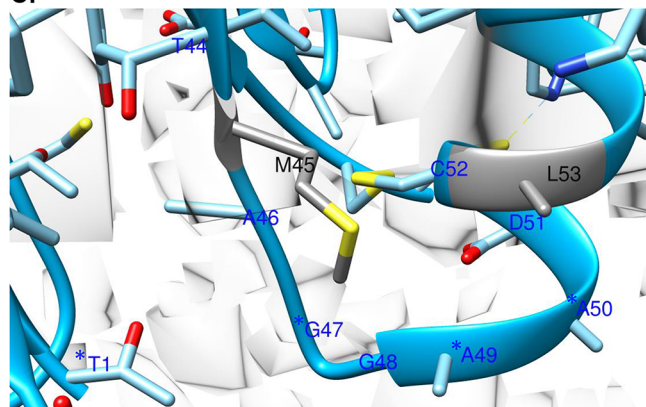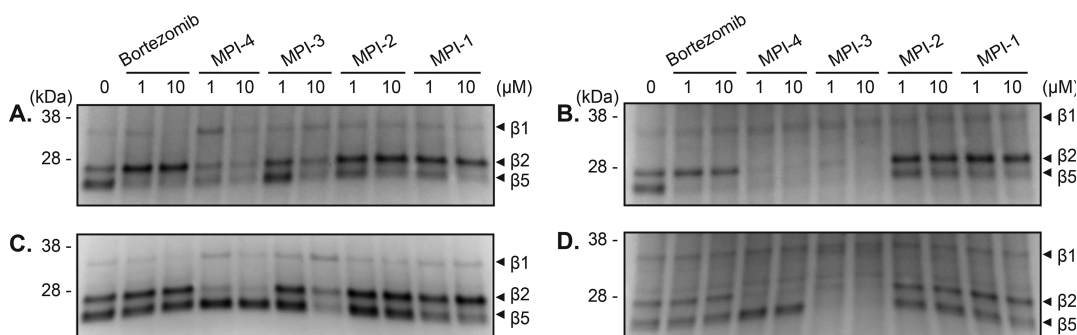

Figure 2. Sequence analysis of bortezomib-resistant parasites. (A) Comparison of sequences of β5 subunits of human and *Pf*20S. Residue positions are calculated at the start of the processed protein, and the first residue (Thr 1) is shown in red and underlined. Mutations that have been selected in human and *P. falciparum* cell lines are highlighted in yellow and green, respectively. (B) Molecular model of β5 subunit of *Pf*20S (PDB code 5fmg) illustrating the Met45 and Leu53 residues that are mutated upon selection for resistance to bortezomib. (C) Mutations are located close to the anticipated bortezomib-binding pocket. Met45 and Leu53 residues are colored in gray. Residues shown in bold and underlined in (A) or marked with asterisks (T1, G47, A49, and A50) in (C) are identical in the yeast and human proteasome β5 subunit and/or have been shown to form direct hydrogen bonding interactions with bortezomib.[22,33]

than clone B2a. This additional mutation is located close to Met45 in the proteasome structure. A mutation in Cys52 (which lies adjacent to the Leu53 residue in *P. falciparum*) has been observed in human cell lines selected for bortezomib. The Leu53Phe mutation places a bulky hydrophobic group close to the P1 pocket of *Pf*20S β5 (Figure S5D) and may cause additional alterations in the local conformation of the active site that inhibit bortezomib binding. Taken together, these data confirm that the β5 activity of the *P. falciparum* proteasome is the main target of bortezomib.

We examined the abilities of the novel compounds to inhibit the growth of the bortezomib-resistant parasite line (B1). The resistant parasites showed very strong cross-resistance to MPI-2 and weaker (2-fold) cross-resistance to MPI-1 (Tables 2A, 3B). Interestingly, the bortezomib-resistant parasite line retained sensitivity to compounds MPI-3 and MPI-4,

suggesting that co-inhibition of β2 activity can overcome the resistance phenotype. This is consistent with a recent study[11] that revealed marked synergism of inhibitors of *Pf*20S β2 and β5. The resource of bortezomib resistant parasites will provide a valuable underpinning for further efforts to design and validate inhibitors.

Active Site Probe Analysis of Proteasome Subunit Specificity. A fluorescent activity probe (BMV037) contains an epoxyketone peptidic scaffold based on carfilzomib.[37,38] We synthesized BMV037 using a procedure modified from the published method[38] (see Supporting Information). We treated purified *Pf*20S (Figure 3A) or intact *P. falciparum* (Figure 3B) with different concentrations of the novel compounds. Residual proteasome activity in the treated purified *Pf*20S or in lysates generated from the treated intact *P. falciparum*-infected erythrocytes was detected using BMV037. In the

Figure 3. Active site probe analysis of the proteasome subunit specificity of the selected compounds in 3D7 parent and bortezomib-resistant parasites. Purified *Pf*20S proteasome from wild-type 3D7 (A) and bortezomib-resistant (C) parasites or wild-type 3D7 (B) and bortezomib-resistant (D) trophozoite-infected erythrocytes were treated with compounds for 1 h, and activity-based probe (BMV037) labeling was performed (postlysis for the trophozoite samples). Fluorescent gel scans reveal subunits that remain active after treatment.

absence of inhibitors, the β5 and β2 subunits are labeled most efficiently, with label also incorporated into the β1 subunit (Figure 3A,B, left lanes), consistent with previous reports.[37,38] Upon treatment of infected erythrocytes with bortezomib, preferential inhibition of the β5 activity is observed (as indicated by an increase in the ratio of β2 to β5 labeling), with some inhibition of β1 activity (Figure 3A). This is consistent with activity assay results for the purified proteasome (Table 1) and similar to the profile of inhibition in human cells.[21] Similarly, MPI-1 and MPI-2 preferentially inhibited binding of the probe to the β5 subunit. By contrast, MPI-3 and MPI-4 inhibited both β2 and β5 activities (Figure 3A,B).

We next analyzed the specificity of the compounds against the active sites in purified human 20S proteasome preparations (Figure S6). BMV037 was incorporated into all the catalytic sites of human constitutive proteasome and immuno-proteasome (Figure S6, left lanes), with a labeling profile similar to that observed in previous studies.[39,40] In agreement with the inhibitory activities assessed using the fluorogenic assay (Table 1B,C), bortezomib preferentially inhibits the β1 and β5 subunits of the human constitutive proteasome and immunoproteasome (Figure S6). Similarly, MPI-3 and MPI-4 exhibited preferential inhibition of the β1 and β5 subunits. Interestingly, despite MPI-3 exhibiting a low IC$_{50}$ value (9 nM) against β5 activity (Table 1B), labeling of the human β1 and β5 subunits was still evident after the treatment with 1 μM MPI-3, especially for the constitutive proteasome. This could be caused by the higher reversibility of MPI-3. MPI-2 preferentially inhibited β1c and β5i and was the only compound that displayed differential inhibition of the constitutive proteasome and immunoproteasome. This differential specificity was not observed in the fluorogenic assay, probably due to the small differences in IC$_{50}$ values (<5-fold) between β1 and β5 sites. MPI-1 preferentially targeted the β5 subunits of both the constitutive proteasome and immunoproteasome but did not completely ablate binding of the probe to β5c, even at a concentration of 10 μM, again suggesting reversibility of binding.

We examined the activity probe profile in bortezomib-resistant parasites. In the absence of inhibitors, BMV037 labeled all three subunits (Figure 3C,D), indicating that the carfilzomib-based probe is still able to bind, despite the changes to the β5 active site. As anticipated, bortezomib was unable to prevent binding of the probe in the resistant parasites, consistent with decreased binding of bortezomib to β5. The competition profile for MPI-3 was very similar in the

bortezomib-resistant and wild-type parasites (compare Figure 3A and Figure 3C), consistent with the maintenance of activity of this compound against bortezomib-resistant parasites. Similarly, MPI-1 was still able to prevent BMV037 labeling of the β5 active site, consistent with the maintenance of substantive killing activity, while MPI-2 was no longer able to prevent BMV037 labeling of the β5 active site, consistent with the loss of parasite killing activity. Of particular interest, MPI-4 was able to completely inhibit BMV037 labeling of the β2 active site but did not prevent labeling of the β5 active site. This suggests that MPI-4 occupancy of the β5 active site is decreased. The maintenance of activity of this compound against bortezomib-resistant parasites suggests that strong inhibition of the β2 active site (plus potentially weaker, reversible inhibition of β5 activity) is sufficient for parasite killing. This is consistent with a previous study[41] showing that inhibitor occupancy of β2 can potentiate proteasome inhibition by weaker inhibitor binding to β5. This insight will guide efforts to generate inhibitors that are more refractory to the development of resistance.

Interestingly, a recent study examined the activity of AsnEDA β5 inhibitor[11] and proposed the extension of the inhibitor to the S4 pocket which is solvent-exposed and formed by amino acid residues of β6. This points to different modes of binding that can be exploited to further enhance specificity. For example, extending the peptidyl boronic acid structures so that they access this pocket could result in improved activity.

Proteasome Substrate Profiling. To determine differences in substrate preference that could be exploited in further development of inhibitors that specifically target the *P. falciparum* proteasome, we screened a large library of AMC-based discrete tripeptide substrates (i.e., 5920 of 8800 theoretical Ac-P3-P2-P1-AMC substrates).[42] Positions adjacent to the cleavage site are referred to as the P3, P2, and P1 positions (Figures 4A−C and S7A,B). The majority of the substrates are preferentially cleaved by the human constitutive proteasome and immunoproteasome (compare Figure 4A, Figure 4B, and Figure S7A). The profile is generally less active and narrower for *Pf*20S; however, residues in some positions do confer some specificity toward *Pf*20S.

Interestingly, *Pf*20S activity is enhanced for substrates with tryptophan (W) at both the P2 and P3 positions (Figure 4A). By contrast, human 20S exhibited poor selectivity at P2 but also preferred tryptophan at P3 position (Figures 4B and S7A). In human 20S, preference for tryptophan at P2 generally results from β2 or β5 activity, while it may select for β1 and β2
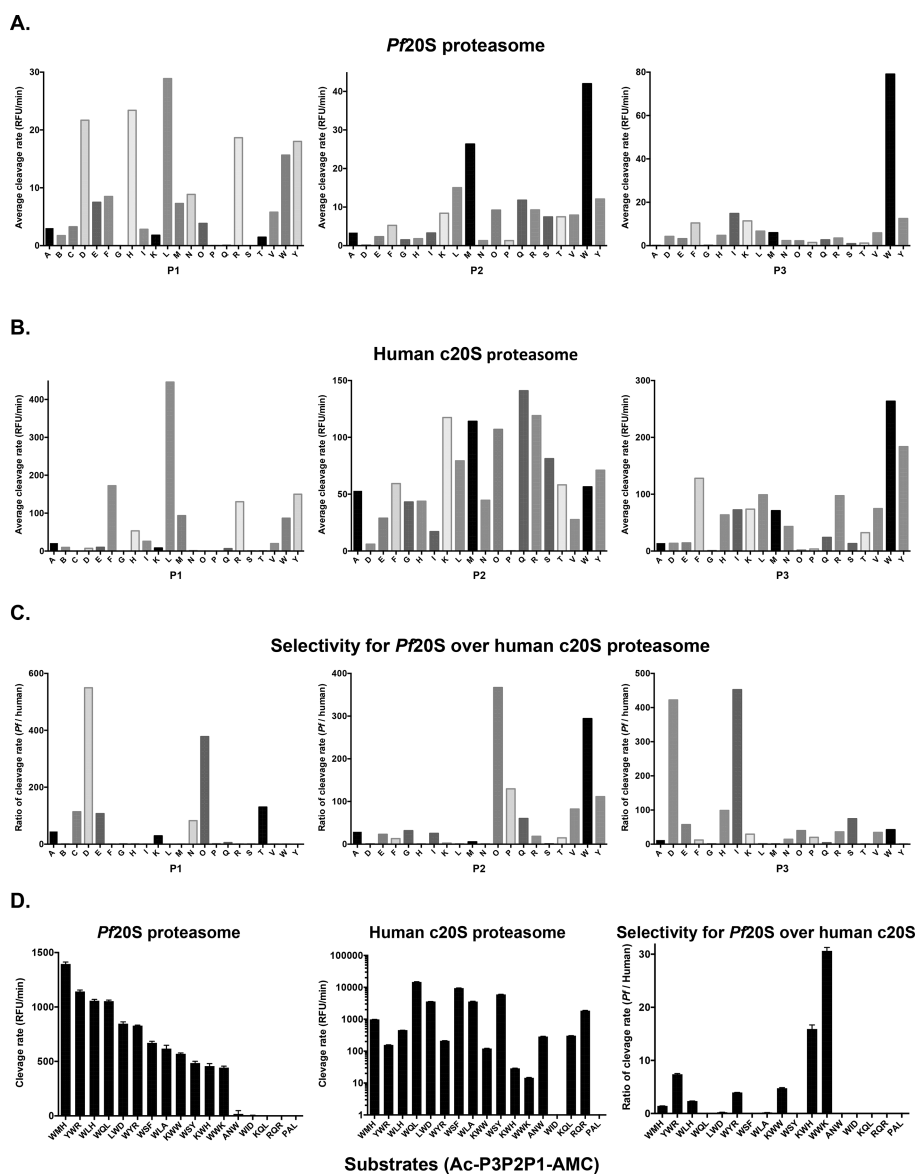
Figure 4. *Pf*20S and human 20S constitutive (c20S) proteasome substrate profiling and validation of active and selective substrates for *P. falciparum* proteasome. Human and *P. falciparum* proteasome activity was measured using a library of AMC-based tripeptide substrates to determine cleavage preferences for each P position. Substrate specificity at P1, P2, and P3 positions was examined for *Pf*20S (A) and human constitutive (B) proteasomes. The *Y*-axis shows the average cleavage rate. Correlation between substrate sequence at each position and average cleavage activity by the proteasome is displayed. Cleavage rate for each substrate is normalized to Ac-WLR-AMC activity (×1000). B indicates either aspartic acid or asparagine. O is pyrrolysine. (C) Selectivity for *Pf*20S proteasome compared with human constitutive proteasome. The ratio of *Pf*20S to human constitutive proteasome cleavage activity is plotted based on the residues at P1, P2, and P3 positions. (D) Validation of selected substrates with *Pf*20S and human constitutive proteasomes. The cleavage rate for each substrate is normalized to Ac-WLR-AMC activity (×1000). Data shown are the mean ± SEM from three independent experiments.

when it is at the P3 position. Aspartic acid (D), leucine (L), histidine (H), tryptophan (W), arginine (R), and tyrosine (Y) are all favored by *Pf*20S at the P1 position (Figure 4A). The data are somewhat different from a previous study,[13] which suggested that *Pf*20S prefers aromatic residues at P1 and P3 due to the more open conformation of the β2-binding pocket compared to the human proteasome. Our data suggest a broader preference profile at P1 and a preference for tryptophan at P3, but the preference for tyrosine or phenylalanine is not as pronounced. Substrate preferences for human constitutive proteasome and immunoproteasome were very similar (Figures 4B and S7A). The only apparent difference was the increased tolerance of large hydrophobic

residues (i.e., F, W, Y) by the immunoproteasome at the P1 and P2 positions.

Because the proteasome harbors three different catalytic sites, it is difficult to pinpoint which β subunit is responsible for the cleavage of a particular substrate. Our *Pf*20S substrate profiling method has the advantage that P2 and P3 preferences can be assigned to a particular P1 residue and has previously been used to profile several other mammalian and bacterial proteasomes.[43] It also can identify individual peptides with especially high activity or selectivity for one active site versus another, whereas these trends may be muted in pooled library approaches. Such substrates can be used directly in further biochemical assays.[43]

Differences in the substrate profiles of *Pf*20S and human constitutive 20S are illustrated by the correlation plot of the substrate library (Figure S8), with many of the selective substrates associated with a high rate of cleavage by their respective targets. The *Pf*20S P3 preference for tryptophan (for β2 and β5) favors substrates such as WLR and WLA, while *Pf*20S P2 preference for tryptophan (for β1 and β2) favors substrates such as DWD and YWR. *Pf*20S β5 (P1 hydrophobic) strongly prefers P3 tryptophan over similar aromatic residues (such as phenylalanine/tyrosine) at P3 (e.g., WQL vs FQL, YQL). This overlaps with human 20S β5 specificity, which is permissive of these alternative P3 residues. *Pf*20S β2 (P1 basic) prefers P1 arginine over lysine with aromatic residues in P2 and P3 (e.g., FWR, YWR). In contrast, for human 20S, if P1 is basic (β2), a basic residue is also preferred at P3 with little selectivity in P2 (e.g., RQR, RLR), with KQY also favored, while if P1 is hydrophobic (β5), an aromatic residue is preferred at P3 (e.g., WLA). *Pf*20S β1 (P1 acidic) appears to have selectivity for hydrophobic or aromatic P2 or P3 residues. Several P1 His substrates (e.g., KWH, WMH) cannot be definitively ascribed to a particular subunit but appear highly active and selective for *Pf*20S. Taken together, these results suggest that significant differences exist between *Pf* 20S and human 20S, which might be exploited in the design of selective *Pf*20S inhibitors.

Overall, the substrate profiling results are similar to a previous study[13] but with some important differences. The selectivity of *Pf*20S for tryptophan in P3 is consistent across the studies, but the preferred residue at P2 (W, M, Y) does not match well with the previous report,[13] possibly due to poor selectivity in P2. The rank order of P1 preferred residues roughly corresponds to the previous report.

To validate these substrate preferences, we resynthesized a number of differentiating substrates based on their activity and selectivity for the *Pf*20S proteasome and directly compared their relative activities as substrates for *Pf*20S proteasome, human 20S constitutive proteasome, and immunoproteasome (Figures 4D and S7C). The preference of *Pf*20S for histidine and arginine in P1 was confirmed, as well as the preference for tryptophan at P2 and P3. It is important to consider residue preferences at different position as a combination rather than individual preferences. For example, Ac-RQR-AMC (arginine at P1) is inactive for *Pf*20S but it is a good human proteasome β2 substrate. The preference for aspartate at P1 was not confirmed, possibly due to a problem with the quality of the substrates in the original library. The selectivity of a number of substrates for *Pf*20S was confirmed. For example, Ac-KWH-AMC and Ac-WWK-AMC appear both active and selective for *Pf*20S. Interestingly, both substrates have tryptophan at the P2 position. While the human immunoproteasome is more tolerant of large bulky side groups at P2 than the constitutive proteasome, *Pf*20S retained evident selectivity for these substrates. Thus, the higher inhibitory activity of MPI-3 and MPI-4 against *Pf*20S may reflect their bulky hydrophobic groups at P2 and P3, and the fact that the *Pf*20S β2 site is more hydrophobic than human 20S.[9] While this manuscript was under review, another study was published that used substrate profiling to design optimized vinyl sulfone-based inhibitors.[44] This work suggests that choice of an optimal electrophilic warhead can further enhance selectivity.

CONCLUSIONS

We have identified potent inhibitors of the *P. falciparum* proteasome that have significant activity against both artemisinin-sensitive and -resistant parasites in culture. While preferential inhibition of *P. falciparum* β2 activity was readily achieved, we show that inhibition of *P. falciparum* β5 activity coupled with weaker or reversible activity against human β5 activity represents a signature that permits selective killing of *P. falciparum* compared with a mammalian line. We developed resistance to bortezomib in *P. falciparum* and show this is associated with mutations in the β5 active site. These mutations prevent binding of some but not other related peptide boronates, and we show that strong inhibition of the β2 active site permits retention of good antiplasmodial activity even in the context of weaker β5 inhibition. Deployment of proteasome inhibitors antimalarial drugs in combinations with drugs with a different mode of action will help avoid the development of resistance. We identified MPI-1 as a compound with good selectivity between *P. falciparum* and a mammalian cancer cell line and the ability to maintain reasonable activity against the bortezomib-resistant parasite line. We have identified amino acid residues at the P1, P2, and P3 that can confer selective binding to the *P. falciparum* proteasome, providing a path to further modification of the peptide boronate scaffold to generate more selective inhibitors.

EXPERIMENTAL METHODS

General Chemistry. All reagents and solvents were used as obtained. ^{1}H NMR spectra were run on a 400 MHz Bruker spectrometer in the solvent indicated. Full assignment of the NMR peaks can be found in the Supporting Information (Figure S9). LC/MS spectra were recorded on an LC or UPLC system connected to a mass spectrometer using reverse phase C18 columns. Various gradients and run times were selected in order to best characterize the compounds. Mobile phases were based on ACN/water or MeOH/water gradients and contained either 0.1% formic acid or 10 mM ammonium acetate (typical gradients of 100% mobile phase A (mobile phase A = 99% water + 1% ACN + 0.1% formic acid) to 100% mobile phase B (mobile phase B = 95% ACN + 5% water + 0.1% formic acid) at a flow rate of 1 mL/min for a 16.5 min LC run or 0.5 mL/min for a 5 min UPLC run). All compounds were determined to be >95% pure by ^{1}H NMR or LC/MS.

BMV037 Fluorescent Probe. BMV037 was prepared using a modification of the published procedure[38] (see Supporting Information for details). ^{1}H NMR spectra were run on a 400 MHz Varian Inova spectrometer. LC/MS spectra were recorded on an Agilent RP-HPLC system connected to a mass spectrometer using a reverse phase C18 column. Compound purity was assessed using a C18 150 mm × 4.6 mm 5 μm column in gradient mode with eluent (buffer) A, 0.1% aq TFA, and buffer B, 0.1% TFA in ACN.

tert-Butyl ((*S*)-1-Oxo-1-(((*R*)-2-phenyl-1-((3a*S*,4*S*,6*S*,7a*R*)-3a,5,5-trimethylhexahydro-4,6-methanobenzo[*d*][1,3,2]-dioxaborol-2-yl)ethyl)amino)propan-2-yl)carbamate (5). To a solution of (*R*)-2-phenyl-1-((3a*S*,4*S*,6*S*,7a*R*)-3a,5,5-trimethyl-hexahydro-4,6-methanobenzo[*d*][1,3,2]dioxaborol-2-yl)ethanamine 2,2,2-trifluoroacetate[45] (600 mg, 1.45 mmol) in DCM (12 mL) was added Boc-L-alanine (330 mg, 1.74 mmol) followed by triethylamine (1.0 mL, 7.26 mmol), and the mixture was degassed with nitrogen for 5 min. 2,4,6-Tripropyl-1,3,5,2,4,6-trioxatriphosphorinane 2,4,6-trioxide (T3P) in EtOAc (1.67 M, 1.74 mL, 2.90 mmol) was added, and the reaction mixture was stirred at room temperature for 4 h, quenched by addition of saturated NaHCO3, and extracted with DCM three times. The combined organic phases were washed with water and brine. The DCM phase was dried over Na2SO4, and then the suspension was filtered and concentrated to dryness. The residue was purified by silica gel column chromatography, eluting with

MeOH/DCM to give 500 mg (73% yield, 93% purity, LC/MS) of the desired product. ^{1}H NMR (400 MHz, CDCl₃) δ 7.29−7.35 (m, 2 H), 7.19−7.26 (m, 3 H), 6.27−6.48 (m, 1 H), 4.64−4.91 (m, 1 H), 4.29−4.37 (m, 1 H), 4.15−4.27 (m, 1 H), 3.15−3.29 (m, 1 H), 2.96−3.08 (m, 1 H), 2.77−2.87 (m, 1 H), 2.30−2.41 (m, 1 H), 2.13−2.23 (m, 1 H), 1.99−2.05 (m, 1 H), 1.83−1.92 (m, 2 H), 1.41−1.45 (m, 9 H), 1.39−1.41 (m, 3 H), 1.35−1.38 (m, 3 H), 1.29−1.32 (m, 4 H), 0.87 (s, 3 H).

(*S*)-2-Amino-*N*-((*R*)-2-phenyl-1-((3a*S*,4*S*,6*S*,7a*R*)-3a,5,5-trimethylhexahydro-4,6-methanobenzo[*d*][1,3,2]dioxaborol-2-yl)ethyl)propanamide Hydrochloride (6). To a solution of **5** (500 mg, 1.06 mmol) in DCM (7.0 mL) was added a solution of HCl in 1,4-dioxane (4 M, 1 mL, 5.32 mmol) slowly at room temperature, and the reaction mixture was stirred at room temperature for 1 day and then concentrated to dryness. To the residue was added Et₂O, and the mixture was sonicated for 5 min. The resulting mixture was concentrated to dryness to give 400 mg (93% yield, 86% purity, LC/MS) of the desired product. ^{1}H NMR (400 MHz, CD₃OD) δ 7.20−7.32 (m, 5 H), 4.35 (d, *J* = 7.53 Hz, 1 H), 3.88 (d, *J* = 6.90 Hz, 1 H), 2.84−2.99 (m, 2 H), 2.33−2.41 (m, 2 H), 2.10−2.19 (m, 1 H), 1.99 (t, *J* = 5.40 Hz, 1 H), 1.80−1.92 (m, 2 H), 1.45 (d, *J* = 7.15 Hz, 3 H), 1.40 (s, 3 H), 1.31 (s, 3 H), 1.19 (d, *J* = 10.79 Hz, 1 H), 0.86−0.92 (m, 3 H).

(*R*)-1-Acetyl-*N*-((*S*)-1-oxo-1-(((*R*)-2-phenyl-1-((3a*S*,4*S*,6*S*,7a*R*)-3a,5,5-trimethylhexahydro-4,6-methanobenzo[*d*]-[1,3,2]dioxaborol-2-yl)ethyl)amino)propan-2-yl)pyrrolidine-2-carboxamide (7, MPI-1 Pinane Ester). (*R*)-(+)-*N*-Acetylproline (102 mg, 0.65 mmol) and **6** (240 mg, 0.59 mmol) were dissolved in DCM (4.0 mL). To this solution was added triethylamine (0.25 mL, 1.77 mmol), and the mixture was degassed with nitrogen for 5 min. 2,4,6-Tripropyl-1,3,5,2,4,6-trioxatriphosphorinane 2,4,6-trioxide (T3P) in EtOAc (1.67 M, 0.70 mL, 1.18 mmol) was added, and the resulting mixture was stirred at room temperature for 4 h, quenched by addition of saturated NaHCO₃, and extracted with DCM three times. The combined organic phases were washed with water and brine. The DCM phase was dried over Na₂SO₄, and then the suspension was filtered and concentrated to dryness. The residue was purified by reverse phase C18 silica gel column chromatography, eluting with ACN/H₂O with 0.1% formic acid to give 115 mg (38% yield, 100% pure, LC/MS) of the desired product. ^{1}H NMR (400 MHz, CDCl₃) δ 9.44 (br s, 1H), 9.08 (br s, 1H), 7.38 (br d, *J* = 7.58 Hz, 2H), 7.05−7.19 (m, 3H), 4.73−4.86 (m, 1H), 4.09 (br d, *J* = 8.19 Hz, 1H), 3.93−4.03 (m, 1H), 3.51−3.73 (m, 2H), 3.27−3.33 (m, 1H), 3.00−3.12 (m, 1H), 2.74−2.87 (m, 1H), 2.15−2.23 (m, 1H), 2.11−2.15 (m, 1H), 2.08 (s, 3H), 1.93−2.04 (m, 2H), 1.80−1.88 (m, 1H), 1.71−1.80 (m, 1H), 1.65−1.70 (m, 1H), 1.58−1.64 (m, 1H), 1.46 (br s, 3H), 1.41−1.45 (m, 1H), 1.33 (s, 3H), 1.15 (s, 3H), 0.79 (br s, 3H), 0.33−0.50 (m, 1H). ^{13}C NMR (101 MHz, CDCl₃) δ 177.1, 172.6, 169.9, 140.2, 130.1, 127.2, 125.4, 83.2, 75.7, 60.2, 52.6, 48.7, 45.6, 44.0, 39.7, 37.9, 36.9, 35.2, 29.5, 29.4, 27.2, 25.4, 25.1, 24.0, 22.4, 16.3. [α]₍D₎²⁰ −80 (*c* 0.1, MeOH).

General Procedure for the Synthesis of the Pinane Esters of MPI-2, MPI-3, and MPI-4 (Compounds 8, 9, and 10). MPI-2, MPI-3, and MPI-4 pinane esters were synthesized using the same procedures described above or using analogous conditions, for instance, substituting TBTU as a coupling reagent for T3P in steps a and c (Scheme 1). Each compound was prepared using commercial or synthesized pinaneboronates.[45,46]

(*S*)-1-Acetyl-*N*-((*S*)-1-(((*R*)-3-methyl-1-((3a*S*,4*S*,6*S*,7a*R*)-3a,5,5-trimethylhexahydro-4,6-methanobenzo[*d*][1,3,2]-dioxaborol-2-yl)butyl)amino)-1-oxopropan-2-yl)pyrrolidine-2-carboxamide (8, MPI-2 Pinane Ester). ^{1}H NMR (400 MHz, CDCl₃) δ 7.90 (br s, 1H), 7.08 (br d, *J* = 8.07 Hz, 1H), 4.61−4.76 (m, 1H), 4.41 (br t, *J* = 6.17 Hz, 1H), 4.23−4.32 (m, 1H), 3.60−3.75 (m, 1H), 3.46−3.58 (m, 1H), 2.82−2.93 (m, 1H), 2.28−2.35 (m, 1H), 2.12−2.19 (m, 3H), 2.09 (s, 3H), 2.00−2.06 (m, 2H), 1.95−2.00 (m, 1H), 1.87−1.93 (m, 1H), 1.78−1.86 (m, 1H), 1.61−1.76 (m, 1H), 1.34−1.44 (m, 8H), 1.31−1.34 (m, 1H), 1.24−1.30 (m, 3H), 0.81−0.94 (m, 9H). ^{13}C NMR (101 MHz, CDCl₃) δ 175.8, 171.7, 171.6, 84.4, 76.4, 60.6, 51.7, 48.4, 46.2, 40.1, 39.9, 39.8, 38.1,

36.1, 29.0, 28.5, 27.2, 26.3, 25.4, 24.9, 24.1, 23.2, 22.3, 21.7, 16.8. [α]₍D₎²⁰ −88 (*c* 0.1, MeOH). 100% pure, LC/MS.

(*S*)-*N*1-((*S*)-1-(((*R*)-3-Methyl-1-((3a*S*,4*S*,6*S*,7a*R*)-3a,5,5-trimethylhexahydro-4,6-methanobenzo[*d*][1,3,2]dioxaborol-2-yl)butyl)amino)-1-oxo-3-phenylpropan-2-yl)-2-((4-methylphenyl)sulfonamido)-*N*4-neopentylsuccinamide (9, MPI-3 Pinane Ester). ^{1}H NMR (400 MHz, CD₃OD) δ 7.13−7.33 (m, 5H), 6.89−7.03 (m, 2H), 6.64−6.75 (m, 2H), 4.73−4.81 (m, 1H), 4.17−4.27 (m, 1H), 3.34−3.45 (m, 2H), 3.02−3.17 (m, 1H), 2.90−3.02 (m, 1H), 2.62−2.74 (m, 1H), 2.30−2.44 (m, 1H), 2.08−2.22 (m, 1H), 1.92−2.03 (m, 1H), 1.84−1.92 (m, 1H), 1.75−1.84 (m, 1H), 1.48−1.59 (m, 1H), 1.42−1.47 (m, 1H), 1.36−1.42 (m, 3H), 1.28−1.36 (m, 3H), 1.20−1.28 (m, 2H), 0.80−0.95 (m, 9H). ^{13}C NMR (101 MHz, CD₃OD) δ 176.8, 174.4, 157.7, 137.5, 131.3, 130.6, 129.8, 128.2, 127.1, 116.6, 84.5, 77.6, 53.7, 52.9, 42.9, 42.4, 41.7, 41.5, 39.3, 38.9, 37.7, 29.9, 27.9, 27.6, 26.7, 24.7, 23.7, 22.4. 100% pure, LC/MS.

(*S*)-2-(2-(4-Hydroxyphenyl)acetamido)-*N*-((*R*)-3-methyl-1-((3a*S*,4*S*,6*S*,7a*R*)-3a,5,5-trimethylhexahydro-4,6-methanobenzo[*d*][1,3,2]dioxaborol-2-yl)butyl)-3-phenyl-propanamide (10, MPI-4 Pinane Ester). ^{1}H NMR (400 MHz, CD₃OD) δ 7.66 (br d, *J* = 8.19 Hz, 2H), 7.20−7.33 (m, 7H), 4.59 (br t, *J* = 7.15 Hz, 1H), 4.15−4.22 (m, 1H), 4.03 (br t, *J* = 6.42 Hz, 1H), 3.07 (br dd, *J* = 6.60, 13.82 Hz, 1H), 2.85−2.97 (m, 3H), 2.61−2.68 (m, 1H), 2.47−2.57 (m, 1H), 2.41−2.47 (m, 1H), 2.39 (s, 3H), 2.31−2.38 (m, 1H), 2.07−2.18 (m, 1H), 1.92−2.00 (m, 1H), 1.82−1.90 (m, 1H), 1.73−1.82 (m, 1H), 1.53−1.68 (m, 1H), 1.40−1.46 (m, 1H), 1.37 (s, 3H), 1.29 (s, 3H), 1.23−1.28 (m, 2H), 0.82−0.91 (m, 18H). ^{13}C NMR (101 MHz, CD₃OD) δ 176.9, 172.6, 171.7, 145.1, 138.8, 137.7, 130.9, 130.6, 129.9, 128.4, 128.2, 84.4, 77.5, 55.0, 53.7, 53.0, 51.8, 42.7, 41.7, 41.5, 39.6, 39.3, 38.1, 37.8, 33.1, 30.0, 27.9, 27.8, 27.6, 26.6, 24.7, 23.7, 22.6, 21.7. [α]₍D₎²⁰ −47.4 (*c* 0.1, MeOH). 97% pure, LC/MS.

***Plasmodium falciparum* Culture.** *P. falciparum* parasites used in this study were propagated in O+ human erythrocytes (Australian Red Cross Blood Service) in RPMI-1640, supplemented with GlutaMAX, 25 mM HEPES (Thermo Fisher Scientific), 5% (v/v) human serum (Australian Red Cross Blood Service), 0.25% (w/v) AlbuMAX II (Thermo Fisher Scientific), 10 μM D-glucose, 22 μg/mL gentamycin (Sigma-Aldrich), and 0.5 mM hypoxanthine (Sigma-Aldrich) and incubated at 37 °C in an atmosphere of 1% O₂, 5% CO₂, and 94% N₂. Cultures were monitored by Giemsa staining of methanol-fixed blood smears. Culture medium was replaced at least every 48 h, and parasitemia was maintained below 10% to ensure health of cultures. The GFP-DD reporter strain was kindly provided by Dr. Paul Gilson, Dr. Brendan Crabb, and Dr. Mauro F. Azevedo (Burnet Institute).

HCT116 and HepG2 Cell Culture. HCT-116 and HepG2 cells were obtained from the American Type Culture Collection and maintained as recommended by the supplier. Cells were cultured in the ATCC-formulated McCoy's 5A medium or DMEM (Life Technologies, CA), supplemented with fetal bovine serum to a final concentration of 9−10%, and incubated at 37 °C in an atmosphere of 95% air and 5% CO₂. Cellular toxicity assays were performed using Promega's CellTiter-Glo assay system. Varying concentrations of the test compounds in 5% DMSO/95% PBS were dispensed into a 384-well plate and cells added to each well. The plates were incubated at 37 °C for 72 h, and the CellTiter-Glo assay to assess cell viability was performed as described by the manufacturer (Promega).

Assessment of Cellular Toxicity. For standard assays of antiplasmodial activity, sorbitol-treated ring stage parasites were incubated with the drugs for 72 h and viability was assessed in the second cycle.[12] Drug pulse assays were performed as described previously.[47] For short pulse assays, tightly synchronized early ring stage parasites (1−3 h after invasion) at 0.2% hematocrit and 1−2% parasitemia were subjected to 3 h drug pulse at 37 °C and returned to culture until parasites reached trophozoite stage of the following cycle. Cells were then stained with 2 μM Syto-61 (Thermo Fisher Scientific), and their fluorescence was measured by flow cytometry (FACSCanto II cytometer; Becton Dickinson). Data were gated and

analyzed using FCS Express software (version 3) to determine parasitemia of each sample. Viability represents the parasitemia normalized to untreated and "kill treated" controls, where "kill treated" refers to samples treated with 2 μM DHA for 48–72 h. Interactions between DHA and MPI-1 or MPI-4 against the K13 mutant (DHA resistant) Cam3.II *P. falciparum* strain, exposed to a 3 h pulsed treatment, were determined at 4 h after invasion as described previously.[12]

For human cell line activity assays, cellular toxicity assays were performed as described previously.[23,48]

P. falciparum Proteasome Preparation and Assay Optimization. *P. falciparum* 20S proteasome was enriched from infected RBCs using a two-step chromatographic procedure.[9] Mass spectrometry revealed the presence of all 14 *Pf*20S proteasome subunits with multiple unique peptide fragments. To determine the level of human proteasome contamination in the purified samples, 7 μg of the purified *Pf*20S proteasome was reduced with DTT and alkylated with iodoacetamide. The sample was then subjected to SDS–PAGE, and the gel fraction containing 14–38 kDa bends was excised. In-gel digestion with trypsin was performed, and peptide content was analyzed by LC–MS/MS. The data were processed using Proteome Discoverer 1.4 employing a user-defined protein database containing human and *Pf*20S proteasome subunits.

Peptide pairs of human and *Pf*20S subunits with similar amino acid sequences were selected and used to estimate the amount of *P. falciparum* proteasome relative to human proteasome. Signal intensity (peak area) from multiple peptide pairs was determined. The signal intensity ratio of *Pf*20S to human 20S proteasome was 240:1 on average, indicating a level of contamination by human proteasome of less than 0.5%. Human proteasome and human proteasome activator complex, PA28$\alpha\beta$, were prepared as described previously.[49] Optimization experiments indicated that 1 nM *Pf*20S was sufficient to produce a strong and reliable signal in the presence of 24 nM PA28$\alpha\beta$, which was found to activate *Pf*20S maximally.

Proteasome Inhibitor Analysis. Proteasome activity was determined using Ac-nLPnLD-AMC (Bachem) for caspase-like (β1) activity, Ac-WLR-AMC (custom, Anaspec, Freemont, CA) for trypsin-like (β2) activity, and Ac-WLA-AMC (custom, Anaspec, Freemont, CA) for chymotrypsin-like (β5) activity. Compounds with 3-fold dilutions from 10 μM (10 concentration points in duplicate) were plated out into black 1536-well plates. The reaction was initiated by adding the AMC substrates, PA28$\alpha\beta$, and 20S proteasome sequentially to the plates. 1 nM *Pf*20S proteasome, 24 nM PA28$\alpha\beta$, and 15 μM AMC substrates were incubated in the assay buffer (50 mM Tris, 5 mM MgCl$_2$, 1 mM DTT, 0.01% BSA, pH 7.4) at 37 °C for 1 or 2 h. Release of AMC fluorophore (excitation, 360 nm; emission, 450 nm) was measured using a fluorescence microplate reader (FLUOstar, BMG Labtech). Slopes of AMC formation over the measurement period were determined for each compound concentration to assess the inhibitory effect (i.e., end-point assay). The same set of compounds was also tested for inhibitory activity against human 20S constitutive proteasome and immunoproteasome (Boston Biochem).

Labeling of Proteasome Catalytic Subunit by BMV037. *P. falciparum* culture, purified *Pf*20S proteasomes, human constitutive proteasomes, or immunoproteasomes (Boston Biochem) were incubated with test compounds at 37 °C for 1 h. Treated parasite lysates (10 μg), *Pf*20S proteasomes (80 nM), human constitutive proteasomes (20 nM), or immuno-20S proteasomes (20 nM) were labeled with BMV037 (10 μM) at 37 °C for 2 h. Samples were mixed with SDS loading buffer and heated at 95 °C for 5 min. Samples for *P. falciparum* and human immuno-20S were run on 4–12% Bis-Tris acrylamide gels using MES SDS running buffer (Thermo Fisher Scientific). Human constitutive 20S samples were run on a 10% Bis-Tris acrylamide gel using MOPS SDS running buffer (Thermo Fisher Scientific). Gels were imaged at the Cy5 channel on a Gel Doc XR+ Documentation System (Bio-Rad) or an Amersham Typhoon Trio imager (GE Healthcare Life Sciences).

Substrate Profiling. 5920 of 8800 theoretical Ac-P3-P2-P1-AMC substrates (2 μL reaction, 20 μM substrate) were assayed in black 1536-well plates with relevant controls: Ac-nLPnLD-AMC (β1), Ac-WLR-AMC (β2), Ac-WLA-AMC (β5). AMC (10 μM) was used as the fluorescence standard. *Pf*20S reaction condition: *Pf*20S (1 nM), human PA28 $\alpha\beta$ (24 nM), in 50 mM Tris, pH 7.5, 5 mM MgCl$_2$, 1 mM DTT, 0.01% BSA. Human 20S reaction condition: 0.25 nM human constitutive proteasome or immunoproteasome (Boston Biochem), PA28 $\alpha\beta$ (24 nM) in 20 mM HEPES, pH 7.4, 0.5 mM EDTA, 0.01% BSA. The assays were read in kinetic mode at 37 °C using a BMG PHERAstar plate reader, and the rate data were normalized to activity obtained using the Ac-WLR-AMC substrate (=1000 units). For validation of substrate preferences, relevant Ac-P3-P2-P1-AMC substrates were resynthesized by CPC Scientific, CA, USA, and assayed for activity against human and *P. falciparum* 20S proteasomes in 96-well plates (80 μL reaction, 10 μM substrate) under the same reaction condition.

In Silico Analysis. All structure analysis was performed using PyMOL.[36] The structure of human 20S (PDB code 5lf3, chain K) was superimposed onto *P. falciparum* 20S (PDB code 5fmg, chain L). The distances between atoms was measured using the Measurement Wizard feature, with bortezomib remaining in the position modeled by the human 20S bound state. Mutagenesis was performed using the Mutagenesis Wizard feature, with rotamers showing minimal clashes being selected. No energy minimization modeling was performed.

In Vitro Evolution of Resistance to Bortezomib and Whole Genome Sequencing. Prior to selection, an aliquot of the parental line was stocked as a reference for subsequent whole genome sequencing analysis. Several independent clones of *P. falciparum* 3D7 parasite line were cultured in Petri dishes exposed to increasing drug pressure for ∼30 weeks. Parasites were cloned by limiting dilution. For parasite extraction and genomic DNA isolation, cultures were scaled up to at least 4–5% parasitaemia, lysed in saponin, and genomic DNA was isolated using ISOLATE II Genomic DNA kit (Bioline). DNA libraries for each gDNA sample were prepared for sequencing using the Nextera XT kit as described previously.[50] Libraries were clustered and run on an Illumina HiSeq 2500 using the RapidRun mode, sequencing 100 base pairs in depth on either end. Paired-end reads were either aligned to the *P. falciparum* 3D7 reference genome (PlasmoDB version 13.0).

Measurement of GFP-DD Signal Using Flow Cytometry or Western Blotting. Trophozoite-stage parasite cultures (GFP-DD parasites) at 5% hematocrit and 5% parasitemia were subjected to the drug treatment indicated in the figure legends at 37 °C. For flow cytometry analyses, culture samples were stained with 2 μM Syto-61 and adjusted to 0.1% hematocrit in PBS. Syto-61 and GFP fluorescence was recorded using the FACSCanto II cytometer (Becton Dickinson). Analysis was performed in FlowJo (version10). Parasites were gated based on parasite GFP fluorescence, and values reported are mean fluorescence. Data were fit by sigmoidal, nonlinear analyses using GraphPad Prism software. For Western blotting, trophozoite-stage parasites were isolated with 0.05% w/v saponin and pellets were washed in PBS, supplemented with EDTA-free protease inhibitor cocktail (Roche). Parasite pellets were solubilized in reducing SDS–PAGE sample buffer, boiled at 95 °C for 8 min, resolved by SDS–PAGE on a 4–12% Bis-Tris acrylamide gel (Life Technologies) using MOPS running buffer and transferred to nitrocellulose membrane (iBlot; Life Technologies). Membranes were blocked with 3.5% skim milk for 1 h at room temperature and probed with mouse anti-GFP (Roche; 1:1000) or mouse anti-*Pf*BiP (1:1000) overnight at 4 °C, followed by goat anti-mouse IgG-peroxidase (Chemicon-AP127P; 1:20 000) for 1 h at room temperature. Polyclonal mouse anti-*Pf*BiP was generated using recombinant *Pf*BiP at the WEHI Antibody Services. Blots were visualized using Clarity ECL substrate (BioRad).

■ ASSOCIATED CONTENT

Ⓢ Supporting Information

The Supporting Information is available free of charge on the ACS Publications website at DOI: 10.1021/acs.jmedchem.8b01161.

Molecular formula strings and some data (CSV)

Tables S1 and S2 listing sequencing statistics and summary of single nucleotide variants and insertion-deletions for bortezomib resistant *P. falciparum* clones; Figure S1−S9 showing purification of *Pf*20S proteasome; optimization of *Pf*20S proteasome activities; kinetic analysis of MPI-4; in vitro evolution of resistance to bortezomib; structure analysis of β5 mutations associated with bortezomib resistance; active site probe analysis of the selected compounds; proteasome substrate profiling of human 20S immunoproteasome and *P. falciparum* proteasome; substrate preferences of human constitutive and *Pf*20S proteasomes; NMR structural assignments of MPI compounds; synthesis of BMV037 (PDF)

■ AUTHOR INFORMATION

Corresponding Author
*E-mail: ltilley@unimelb.edu.au.

ORCID
Craig A. Hutton: 0000-0002-2353-9258
Elizabeth A. Winzeler: 0000-0002-4049-2113
Leann Tilley: 0000-0001-9910-0199

Author Contributions
∇L.R.D. and L.T. contributed equally. S.C.X., D.L.G., N.J.S., C.T., S.O., S.D., A.E.G., P.H., F.B., X.Y., C.A.H., J.N.B., E.A.W., V.M.A., L.R.D., and L.T. designed the research. S.C.X., D.L.G., N.J.S., S.D., P.H., F.B., and X.Z. performed cellular and biochemical experiments. C.L.C. and C.A.H. synthesized the BMV037 probe. M.R.L., S.O., and E.A.W. performed whole genome sequencing. All authors analyzed data. S.C.X., L.R.D., and L.T. wrote the manuscript, with input from the other authors.

Notes
The authors declare no competing financial interest.

■ ABBREVIATION USED

ACT, artemisinin-based combination therapy; *P. falciparum*, *Plasmodium falciparum*; *P. berghei*, *Plasmodium berghei*; AsnEDA, asparagine ethylenediamine; PA28αβ, proteasome activator 28αβ; Ac-xxx-AMC, acetyl-xxx-7-amino-4-methylcoumarin; MPI, malaria proteasome inhibitor; T3P, 2,4,6-tripropyl-1,3,5,2,4,6-trioxatriphosphorinane-2,4,6-trioxide; EtOAc, ethyl acetate; ACN, acetonitrile; CDCl$_3$, deuterated chloroform; CD$_3$OD, deuterated methanol; LC/MS, liquid chromatography−mass spectrometry; Et$_2$O, diethyl ether; TBTU, *O*-(benzotriazol-1-yl)-*N*,*N*,*N'*,*N'*-tetramethyluronium tetrafluoroborate; β1/2/5c, constitutive proteasome β1/2/5 subunits; β1/2/5i, immunoproteasome β1/2/5 subunits; GFP-DD, green fluorescent protein−destabilization domain; DHA, dihydroartemisinin; HCT116, human colorectal carcinoma cell line; HepG2, human hepatocellular carcinoma cell line; CNV, copy number variant; CryoEM, cryogenic electron microscopy; HEPES, 4-(2-hydroxyethyl)-1-piperazineethanesulfonic acid; RP-HPLC, reversed-phase high-performance liquid chromatography; MOPS, 3-(*N*-morpholino)propanesulfonic acid; BiP, binding immunoglobulin protein; Et$_3$N, triethylamine

■ REFERENCES

(1) *World Malaria Report 2017*; World Health Organization: Geneva, Switzerland, 2017.

(2) Dondorp, A. M.; Nosten, F.; Yi, P.; Das, D.; Phyo, A. P.; Tarning, J.; Lwin, K. M.; Ariey, F.; Hanpithakpong, W.; Lee, S. J.; Ringwald, P.; Silamut, K.; Imwong, M.; Chotivanich, K.; Lim, P.; Herdman, T.; An, S. S.; Yeung, S.; Singhasivanon, P.; Day, N. P.; Lindegardh, N.; Socheat, D.; White, N. J. Artemisinin resistance in *Plasmodium falciparum* malaria. *N. Engl. J. Med.* 2009, 361, 455−467.

(3) Phyo, A. P.; Nkhoma, S.; Stepniewska, K.; Ashley, E. A.; Nair, S.; McGready, R.; ler Moo, C.; Al-Saai, S.; Dondorp, A. M.; Lwin, K. M.; Singhasivanon, P.; Day, N. P.; White, N. J.; Anderson, T. J.; Nosten, F. Emergence of artemisinin-resistant malaria on the western border of Thailand: a longitudinal study. *Lancet* 2012, 379, 1960−1966.

(4) Amaratunga, C.; Sreng, S.; Suon, S.; Phelps, E. S.; Stepniewska, K.; Lim, P.; Zhou, C.; Mao, S.; Anderson, J. M.; Lindegardh, N.; Jiang, H.; Song, J.; Su, X. Z.; White, N. J.; Dondorp, A. M.; Anderson, T. J.; Fay, M. P.; Mu, J.; Duong, S.; Fairhurst, R. M. Artemisinin-resistant *Plasmodium falciparum* in Pursat province, western Cambodia: a parasite clearance rate study. *Lancet Infect. Dis.* 2012, 12, 851−858.

(5) Amaratunga, C.; Lim, P.; Suon, S.; Sreng, S.; Mao, S.; Sopha, C.; Sam, B.; Dek, D.; Try, V.; Amato, R.; Blessborn, D.; Song, L.; Tullo, G. S.; Fay, M. P.; Anderson, J. M.; Tarning, J.; Fairhurst, R. M. Dihydroartemisinin-piperaquine resistance in *Plasmodium falciparum* malaria in Cambodia: a multisite prospective cohort study. *Lancet Infect. Dis.* 2016, 16, 357−365.

(6) Spring, M. D.; Lin, J. T.; Manning, J. E.; Vanachayangkul, P.; Somethy, S.; Bun, R.; Se, Y.; Chann, S.; Ittiverakul, M.; Sia-ngam, P.; Kuntawunginn, W.; Arsanok, M.; Buathong, N.; Chaorattanakawee, S.; Gosi, P.; Ta-aksorn, W.; Chanarat, N.; Sundrakes, S.; Kong, N.; Heng, T. K.; Nou, S.; Teja-isavadharm, P.; Pichyangkul, S.; Phann, S. T.; Balasubramanian, S.; Juliano, J. J.; Meshnick, S. R.; Chour, C. M.; Prom, S.; Lanteri, C. A.; Lon, C.; Saunders, D. L. Dihydroartemisinin-piperaquine failure associated with a triple mutant including kelch13 C580Y in Cambodia: an observational cohort study. *Lancet Infect. Dis.* 2015, 15, 683−691.

(7) Kisselev, A. F.; van der Linden, W. A.; Overkleeft, H. S. Proteasome inhibitors: an expanding army attacking a unique target. *Chem. Biol.* 2012, 19, 99−115.

(8) Ferrington, D. A.; Gregerson, D. S. Immunoproteasomes: structure, function, and antigen presentation. *Prog. Mol. Biol. Transl Sci.* 2012, 109, 75−112.

(9) Li, H.; Ponder, E. L.; Verdoes, M.; Asbjornsdottir, K. H.; Deu, E.; Edgington, L. E.; Lee, J. T.; Kirk, C. J.; Demo, S. D.; Williamson, K. C.; Bogyo, M. Validation of the proteasome as a therapeutic target in *Plasmodium* using an epoxyketone inhibitor with parasite-specific toxicity. *Chem. Biol.* 2012, 19, 1535−1545.

(10) Tschan, S.; Brouwer, A. J.; Werkhoven, P. R.; Jonker, A. M.; Wagner, L.; Knittel, S.; Aminake, M. N.; Pradel, G.; Joanny, F.; Liskamp, R. M.; Mordmuller, B. Broad-spectrum antimalarial activity

of peptido sulfonyl fluorides, a new class of proteasome inhibitors. *Antimicrob. Agents Chemother.* 2013, 57, 3576−3584.

(11) Kirkman, L. A.; Zhan, W.; Visone, J.; Dziedziech, A.; Singh, P. K.; Fan, H.; Tong, X.; Bruzual, I.; Hara, R.; Kawasaki, M.; Imaeda, T.; Okamoto, R.; Sato, K.; Michino, M.; Alvaro, E. F.; Guiang, L. F.; Sanz, L.; Mota, D. J.; Govindasamy, K.; Wang, R.; Ling, Y.; Tumwebaze, P. K.; Sukenick, G.; Shi, L.; Vendome, J.; Bhanot, P.; Rosenthal, P. J.; Aso, K.; Foley, M. A.; Cooper, R. A.; Kafsack, B.; Doggett, J. S.; Nathan, C. F.; Lin, G. Antimalarial proteasome inhibitor reveals collateral sensitivity from intersubunit interactions and fitness cost of resistance. *Proc. Natl. Acad. Sci. U. S. A.* 2018, 115, E6863−E6870.

(12) Dogovski, C.; Xie, S. C.; Burgio, G.; Bridgford, J.; Mok, S.; McCaw, J. M.; Chotivanich, K.; Kenny, S.; Gnadig, N.; Straimer, J.; Bozdech, Z.; Fidock, D. A.; Simpson, J. A.; Dondorp, A. M.; Foote, S.; Klonis, N.; Tilley, L. Targeting the cell stress response of *Plasmodium falciparum* to overcome artemisinin resistance. *PLoS Biol.* 2015, 13, e1002132.

(13) Li, H.; O'Donoghue, A.; van der Linden, W. A.; Xie, S. C.; Yoo, E.; Foe, I. T.; Tilley, L.; Craik, C. S.; da Fonseca, P. C. A.; Bogyo, M. Structure and function based design of Plasmodium-selective proteasome inhibitors. *Nature* 2016, 530, 233−236.

(14) Kreidenweiss, A.; Kremsner, P. G.; Mordmuller, B. Comprehensive study of proteasome inhibitors against *Plasmodium falciparum* laboratory strains and field isolates from Gabon. *Malar. J.* 2008, 7, 187.

(15) Kumar, S. K.; Berdeja, J. G.; Niesvizky, R.; Lonial, S.; Laubach, J. P.; Hamadani, M.; Stewart, A. K.; Hari, P.; Roy, V.; Vescio, R.; Kaufman, J. L.; Berg, D.; Liao, E.; Di Bacco, A.; Estevam, J.; Gupta, N.; Hui, A. M.; Rajkumar, V.; Richardson, P. G. Safety and tolerability of ixazomib, an oral proteasome inhibitor, in combination with lenalidomide and dexamethasone in patients with previously untreated multiple myeloma: an open-label phase 1/2 study. *Lancet Oncol.* 2014, 15, 1503−1512.

(16) Gupta, N.; Zhao, Y.; Hui, A. M.; Esseltine, D. L.; Venkatakrishnan, K. Switching from body surface area-based to fixed dosing for the investigational proteasome inhibitor ixazomib: a population pharmacokinetic analysis. *Br. J. Clin. Pharmacol.* 2015, 79, 789−800.

(17) Gupta, N.; Yang, H.; Hanley, M. J.; Zhang, S.; Liu, R.; Kumar, S.; Richardson, P. G.; Skacel, T.; Venkatakrishnan, K. Dose and schedule selection of the oral proteasome inhibitor Ixazomib in relapsed/refractory multiple myeloma: Clinical and model-based analyses. *Target Oncol.* 2017, 12, 643−654.

(18) Reynolds, J. M.; El Bissati, K.; Brandenburg, J.; Gunzl, A.; Mamoun, C. B. Antimalarial activity of the anticancer and proteasome inhibitor bortezomib and its analog ZL3B. *BMC Clin. Pharmacol.* 2007, 7, 13.

(19) Pereira, P. H. S.; Curra, C.; Garcia, C. R. S. Ubiquitin proteasome system as a potential drug target for malaria. *Curr. Top. Med. Chem.* 2018, 18, 315−320.

(20) Duffy, S.; Avery, V. M. Development and optimization of a novel 384-well anti-malarial imaging assay validated for high-throughput screening. *Am. J. Trop. Med. Hyg.* 2012, 86, 84−92.

(21) Blackburn, C.; Gigstad, K. M.; Hales, P.; Garcia, K.; Jones, M.; Bruzzese, F. J.; Barrett, C.; Liu, J. X.; Soucy, T. A.; Sappal, D. S.; Bump, N.; Olhava, E. J.; Fleming, P.; Dick, L. R.; Tsu, C.; Sintchak, M. D.; Blank, J. L. Characterization of a new series of non-covalent proteasome inhibitors with exquisite potency and selectivity for the 20S beta5-subunit. *Biochem. J.* 2010, 430, 461−476.

(22) Groll, M.; Berkers, C. R.; Ploegh, H. L.; Ovaa, H. Crystal structure of the boronic acid-based proteasome inhibitor bortezomib in complex with the yeast 20S proteasome. *Structure* 2006, 14, 451−456.

(23) Kupperman, E.; Lee, E. C.; Cao, Y.; Bannerman, B.; Fitzgerald, M.; Berger, A.; Yu, J.; Yang, Y.; Hales, P.; Bruzzese, F.; Liu, J.; Blank, J.; Garcia, K.; Tsu, C.; Dick, L.; Fleming, P.; Yu, L.; Manfredi, M.; Rolfe, M.; Bolen, J. Evaluation of the proteasome inhibitor MLN9708 in preclinical models of human cancer. *Cancer Res.* 2010, 70, 1970−1980.

(24) Banaszynski, L. A.; Chen, L. C.; Maynard-Smith, L. A.; Ooi, A. G.; Wandless, T. J. A rapid, reversible, and tunable method to regulate protein function in living cells using synthetic small molecules. *Cell* 2006, 126, 995−1004.

(25) Ariey, F.; Witkowski, B.; Amaratunga, C.; Beghain, J.; Langlois, A. C.; Khim, N.; Kim, S.; Duru, V.; Bouchier, C.; Ma, L.; Lim, P.; Leang, R.; Duong, S.; Sreng, S.; Suon, S.; Chuor, C. M.; Bout, D. M.; Menard, S.; Rogers, W. O.; Genton, B.; Fandeur, T.; Miotto, O.; Ringwald, P.; Le Bras, J.; Berry, A.; Barale, J. C.; Fairhurst, R. M.; Benoit-Vical, F.; Mercereau-Puijalon, O.; Menard, D. A molecular marker of artemisinin-resistant *Plasmodium falciparum* malaria. *Nature* 2014, 505, 50−55.

(26) Straimer, J.; Gnadig, N. F.; Witkowski, B.; Amaratunga, C.; Duru, V.; Ramadani, A. P.; Dacheux, M.; Khim, N.; Zhang, L.; Lam, S.; Gregory, P. D.; Urnov, F. D.; Mercereau-Puijalon, O.; Benoit-Vical, F.; Fairhurst, R. M.; Menard, D.; Fidock, D. A. Drug resistance. K13-propeller mutations confer artemisinin resistance in *Plasmodium falciparum* clinical isolates. *Science* 2015, 347, 428−431.

(27) Yu, J.; Tiwari, S.; Steiner, P.; Zhang, L. Differential apoptotic response to the proteasome inhibitor Bortezomib [VELCADE, PS-341] in Bax-deficient and p21-deficient colon cancer cells. *Cancer Biol. Ther* 2003, 2, 694−699.

(28) Baragana, B.; Hallyburton, I.; Lee, M. C.; Norcross, N. R.; Grimaldi, R.; Otto, T. D.; Proto, W. R.; Blagborough, A. M.; Meister, S.; Wirjanata, G.; Ruecker, A.; Upton, L. M.; Abraham, T. S.; Almeida, M. J.; Pradhan, A.; Porzelle, A.; Luksch, T.; Martinez, M. S.; Luksch, T.; Bolscher, J. M.; Woodland, A.; Norval, S.; Zuccotto, F.; Thomas, J.; Simeons, F.; Stojanovski, L.; Osuna-Cabello, M.; Brock, P. M.; Churcher, T. S.; Sala, K. A.; Zakutansky, S. E.; Jimenez-Diaz, M. B.; Sanz, L. M.; Riley, J.; Basak, R.; Campbell, M.; Avery, V. M.; Sauerwein, R. W.; Dechering, K. J.; Noviyanti, R.; Campo, B.; Frearson, J. A.; Angulo-Barturen, I.; Ferrer-Bazaga, S.; Gamo, F. J.; Wyatt, P. G.; Leroy, D.; Siegl, P.; Delves, M. J.; Kyle, D. E.; Wittlin, S.; Marfurt, J.; Price, R. N.; Sinden, R. E.; Winzeler, E. A.; Charman, S. A.; Bebrevska, L.; Gray, D. W.; Campbell, S.; Fairlamb, A. H.; Willis, P. A.; Rayner, J. C.; Fidock, D. A.; Read, K. D.; Gilbert, I. H. A novel multiple-stage antimalarial agent that inhibits protein synthesis. *Nature* 2015, 522, 315−320.

(29) Gamo, F. J.; Sanz, L. M.; Vidal, J.; de Cozar, C.; Alvarez, E.; Lavandera, J. L.; Vanderwall, D. E.; Green, D. V.; Kumar, V.; Hasan, S.; Brown, J. R.; Peishoff, C. E.; Cardon, L. R.; Garcia-Bustos, J. F. Thousands of chemical starting points for antimalarial lead identification. *Nature* 2010, 465, 305−310.

(30) LaMonte, G.; Lim, M. Y.; Wree, M.; Reimer, C.; Nachon, M.; Corey, V.; Gedeck, P.; Plouffe, D.; Du, A.; Figueroa, N.; Yeung, B.; Bifani, P.; Winzeler, E. A. Mutations in the *Plasmodium falciparum* Cyclic Amine Resistance Locus (PfCARL) confer multidrug resistance. *mBio* 2016, 7, e00696-16.

(31) Flannery, E. L.; Fidock, D. A.; Winzeler, E. A. Using genetic methods to define the targets of compounds with antimalarial activity. *J. Med. Chem.* 2013, 56, 7761−7771.

(32) Schrader, J.; Henneberg, F.; Mata, R. A.; Tittmann, K.; Schneider, T. R.; Stark, H.; Bourenkov, G.; Chari, A. The inhibition mechanism of human 20S proteasomes enables next-generation inhibitor design. *Science* 2016, 353, 594−598.

(33) Franke, N. E.; Niewerth, D.; Assaraf, Y. G.; van Meerloo, J.; Vojtekova, K.; van Zantwijk, C. H.; Zweegman, S.; Chan, E. T.; Kirk, C. J.; Geerke, D. P.; Schimmer, A. D.; Kaspers, G. J.; Jansen, G.; Cloos, J. Impaired bortezomib binding to mutant beta5 subunit of the proteasome is the underlying basis for bortezomib resistance in leukemia cells. *Leukemia* 2012, 26, 757−768.

(34) Barrio, S.; Stuhmer, T.; Da-Via, M.; Barrio-Garcia, C.; Lehners, N.; Besse, A.; Cuenca, I.; Garitano-Trojaola, A.; Fink, S.; Leich, E.; Chatterjee, M.; Driessen, C.; Martinez-Lopez, J.; Rosenwald, A.; Beckmann, R.; Bargou, R. C.; Braggio, E.; Stewart, A. K.; Raab, M. S.; Einsele, H.; Kortum, K. M. Spectrum and functional validation of PSMB5 mutations in multiple myeloma. *Leukemia* 2018, DOI: 10.1038/s41375-018-0216-8.

(35) LaMonte, G. M.; Almaliti, J.; Bibo-Verdugo, B.; Keller, L.; Zou, B. Y.; Yang, J.; Antonova-Koch, Y.; Orjuela-Sanchez, P.; Boyle, C. A.; Vigil, E.; Wang, L.; Goldof, G. M.; Gerwick, L.; O'Donoghue, A. J.; Winzeler, E. A.; Gerwick, W. H.; Ottilie, S. Development of a potent inhibitor of the Plasmodium proteasome with reduced mammalian toxicity. *J. Med. Chem.* **2017**, *60*, 6721−6732.

(36) *The PyMOL Molecular Graphics System*, version 1.8; Schrödinger, 2015.

(37) Verdoes, M.; Florea, B. I.; Menendez-Benito, V.; Maynard, C. J.; Witte, M. D.; van der Linden, W. A.; van den Nieuwendijk, A. M.; Hofmann, T.; Berkers, C. R.; van Leeuwen, F. W.; Groothuis, T. A.; Leeuwenburgh, M. A.; Ovaa, H.; Neefjes, J. J.; Filippov, D. V.; van der Marel, G. A.; Dantuma, N. P.; Overkleeft, H. S. A fluorescent broad-spectrum proteasome inhibitor for labeling proteasomes in vitro and in vivo. *Chem. Biol.* **2006**, *13*, 1217−1226.

(38) Li, H.; van der Linden, W. A.; Verdoes, M.; Florea, B. I.; McAllister, F. E.; Govindaswamy, K.; Elias, J. E.; Bhanot, P.; Overkleeft, H. S.; Bogyo, M. Assessing subunit dependency of the Plasmodium proteasome using small molecule inhibitors and active site probes. *ACS Chem. Biol.* **2014**, *9*, 1869−1876.

(39) Li, H.; O'Donoghue, A. J.; van der Linden, W. A.; Xie, S. C.; Yoo, E.; Foe, I. T.; Tilley, L.; Craik, C. S.; da Fonseca, P. C.; Bogyo, M. Structure- and function-based design of Plasmodium-selective proteasome inhibitors. *Nature* **2016**, *530*, 233−236.

(40) de Bruin, G.; Xin, B. T.; Kraus, M.; van der Stelt, M.; van der Marel, G. A.; Kisselev, A. F.; Driessen, C.; Florea, B. I.; Overkleeft, H. S. A set of sctivity-based probes to visualize human (immuno)-proteasome activities. *Angew. Chem., Int. Ed.* **2016**, *55*, 4199−4203.

(41) Kraus, M.; Bader, J.; Geurink, P. P.; Weyburne, E. S.; Mirabella, A. C.; Silzle, T.; Shabaneh, T. B.; van der Linden, W. A.; de Bruin, G.; Haile, S. R.; van Rooden, E.; Appenzeller, C.; Li, N.; Kisselev, A. F.; Overkleeft, H.; Driessen, C. The novel beta2-selective proteasome inhibitor LU-102 synergizes with bortezomib and carfilzomib to overcome proteasome inhibitor resistance of myeloma cells. *Haematologica* **2015**, *100*, 1350−1360.

(42) Sheppeck, J. E., 2nd; Kar, H.; Gosink, L.; Wheatley, J. B.; Gjerstad, E.; Loftus, S. M.; Zubiria, A. R.; Janc, J. W. Synthesis of a statistically exhaustive fluorescent peptide substrate library for profiling protease specificity. *Bioorg. Med. Chem. Lett.* **2000**, *10*, 2639−2642.

(43) Lin, G.; Tsu, C.; Dick, L.; Zhou, X. K.; Nathan, C. Distinct specificities of *Mycobacterium tuberculosis* and mammalian proteasomes for N-acetyl tripeptide substrates. *J. Biol. Chem.* **2008**, *283*, 34423−34431.

(44) Yoo, E.; Stokes, B. H.; de Jong, H.; Vanaerschot, M.; Kumar, T.; Lawrence, N.; Njoroge, M.; Garcia, A.; Van der Westhuyzen, R.; Momper, J. D.; Ng, C. L.; Fidock, D. A.; Bogyo, M. Defining the determinants of specificity of *Plasmodium* proteasome inhibitors. *J. Am. Chem. Soc.* **2018**, *140*, 11424−11437.

(45) Kostova, M. B.; Rosen, D. M.; Chen, Y.; Mease, R. C.; Denmeade, S. R. Structural optimization, biological evaluation, and application of peptidomimetic prostate specific antigen inhibitors. *J. Med. Chem.* **2013**, *56*, 4224−4235.

(46) Pickersgill, I. F.; Bishop, J.; Koellner, C.; Gomez, J.-M.; Geiser, A.; Hett, R.; Ammoscato, V.; Munk, S.; Lo, Y.; Chui, F.-T.; Kulkarni, V. R. Synthesis Of Boronic Ester And Acid Compounds. Patent Publication Number WO 2005/097809, 2005; Millenium Pharmaceuticals Inc.

(47) Xie, S. C.; Dogovski, C.; Kenny, S.; Tilley, L.; Klonis, N. Optimal assay design for determining the in vitro sensitivity of ring stage *Plasmodium falciparum* to artemisinins. *Int. J. Parasitol.* **2014**, *44*, 893−899.

(48) Cowell, A. N.; Istvan, E. S.; Lukens, A. K.; Gomez-Lorenzo, M. G.; Vanaerschot, M.; Sakata-Kato, T.; Flannery, E. L.; Magistrado, P.; Owen, E.; Abraham, M.; LaMonte, G.; Painter, H. J.; Williams, R. M.; Franco, V.; Linares, M.; Arriaga, I.; Bopp, S.; Corey, V. C.; Gnadig, N. F.; Coburn-Flynn, O.; Reimer, C.; Gupta, P.; Murithi, J. M.; Moura, P. A.; Fuchs, O.; Sasaki, E.; Kim, S. W.; Teng, C. H.; Wang, L. T.; Akidil, A.; Adjalley, S.; Willis, P. A.; Siegel, D.; Tanaseichuk, O.; Zhong, Y.; Zhou, Y.; Llinas, M.; Ottilie, S.; Gamo, F. J.; Lee, M. C. S.; Goldberg, D. E.; Fidock, D. A.; Wirth, D. F.; Winzeler, E. A. Mapping the malaria parasite druggable genome by using *in vitro* evolution and chemogenomics. *Science* **2018**, *359*, 191−199.

(49) Williamson, M. J.; Blank, J. L.; Bruzzese, F. J.; Cao, Y.; Daniels, J. S.; Dick, L. R.; Labutti, J.; Mazzola, A. M.; Patil, A. D.; Reimer, C. L.; Solomon, M. S.; Stirling, M.; Tian, Y.; Tsu, C. A.; Weatherhead, G. S.; Zhang, J. X.; Rolfe, M. Comparison of biochemical and biological effects of ML858 (salinosporamide A) and bortezomib. *Mol. Cancer Ther.* **2006**, *5*, 3052−3061.

(50) Lim, M. Y.; LaMonte, G.; Lee, M. C.; Reimer, C.; Tan, B. H.; Corey, V.; Tjahjadi, B. F.; Chua, A.; Nachon, M.; Wintjens, R.; Gedeck, P.; Malleret, B.; Renia, L.; Bonamy, G. M.; Ho, P. C.; Yeung, B. K.; Chow, E. D.; Lim, L.; Fidock, D. A.; Diagana, T. T.; Winzeler, E. A.; Bifani, P. UDP-galactose and acetyl-CoA transporters as Plasmodium multidrug resistance genes. *Nat. Microbiol.* **2016**, *1*, 16166.

Author/s:
Xie, SC; Gillett, DL; Spillman, NJ; Tsu, C; Luth, MR; Ottilie, S; Duffy, S; Gould, AE; Hales, P; Seager, BA; Charron, CL; Bruzzese, F; Yang, X; Zhao, X; Huang, S-C; Hutton, CA; Burrows, JN; Winzeler, EA; Avery, VM; Dick, LR; Tilley, L

Title:
Target Validation and Identification of Novel Boronate Inhibitors of the Plasmodium falciparum Proteasome

Date:
2018-11-22

Persistent Link:
http://hdl.handle.net/11343/223064

File Description:
Published version